A Forensic Analysis of "Rubber Duck," a Publicly Available Video Showing a UAP Purportedly Filmed by Arizona National Guard on November 23, 2019

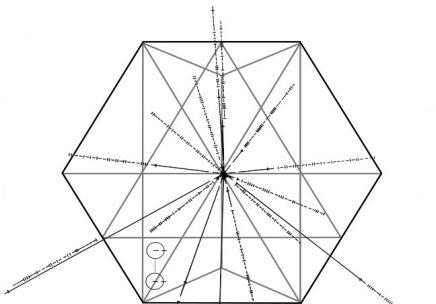

ANALYSIS OF EVIDENCE AND RESULTING CONCLUSIONS

THE SCIENTIFIC COALITION FOR UAP STUDIES

November 12, 2022

Table of Contents

A Forensic Analysis of "Rubber Duck," a Publicly Available Video Showing a UAP Purportedly Filmed by Arizona National Guard on November 23, 2019

Peter Reali[1] *

[1]*Scientific Coalition for UAP Studies, Town Lake Dr., Ste A, #173, Fort Myers, Florida*

*Corresponding author: Peter Reali (scu.project.director@gmail.com)

Abstract:

A multi-faceted, forensic-type analysis was conducted of what has been termed the "Rubber Duck" videos. These are two publicly available .mp4 files that appear to show an unidentified aerospace phenomenon (UAP) moving with no means of propulsion or aerodynamic means of lift across a desert environment. These two, 30 min clips, "Rubber Duck 1 & 2", are claimed to be from an anonymous source at the Department of Homeland Security. They were purportedly taken from a FLIR camera system onboard a RC-26B aircraft used by the Arizona Air National Guard on November 23, 2019. Data displayed on both videos are consistent with video being taken while in flight over the route described by the source. SCU was provided these videos by podcaster Andy Marcial. Kinematics, trajectory, rotation, flight characteristics (including parallax), lighting and temperature are investigated, as well as environmental weather conditions. The results of this analysis support the conclusion that the object cannot be explained as any known natural phenomenon or by any known technology used for aeronautical propulsion. As such, the object can be classified as a UAP. Such objects can be a hazard to aerial transportation, a dangerous distraction to pilots in certain situations, and are worthy of scientific investigation.

A. Narrative, provenance, and description of the videos:

The SCU was provided two videos from podcaster Andy Marcial who had published them on Youtube. Andy Marcial had obtained the videos from an anonymous member of homeland security and provided the SCU with two. mp4 formatted video files, each of which are 30 minutes in length. The source claims they were taken from a FLIR camera system onboard a RC-26B aircraft used by the Arizona Air National Guard on November 23, 2019. Data displayed on both videos is consistent with video being taken while in flight over the route described by the source. The source has named video files "Rubber Duck 1 & 2" due to object's shape in the videos. These will be referred to as RD1 and RD2.

The SCU takes the position that it has no interest in releasing sensitive or classified data that should not be in the public domain and will redact any information that would compromise this position and has made every effort to adhere to these principles. Since the videos are now in the public domain the SCU decided to conduct research on this incident and release a report to understand the nature of the object in the videos. The sole purpose of The SCU is to provide scientific and rigorous analysis so that valid UAP sightings will prove that these objects are real and worthy of study by the larger scientific establishment.

For those interested in more details about the actual event as relayed by the source to Andy Marcial, a redacted version of his narrative is given in **Appendix F (p. 44)**.

Figure 1: RC26B aircraft with FLIR Video camera mounted on bottom of fuselage.

B. Forensic Method of Analysis:

In this analysis the RD2 video was used as the main source of study as the RD1 has a large portion of the video where the object is not present and the later portion of the video has no special information that is not contained in the RD2 video; so, the author focused the analysis on the RD2 video in detail. Considerations for determining if the object in the RD videos can be classified as anomalous: For a scientific analysis using forensic methods of investigation, we use what's called the "null hypothesis" **[3]** as a guideline for a classification of the object's nature. We use the neutral term "object" to avoid any preconceptions or biases in conducting our investigation. We use the term "anomalous" to mean not explainable in terms of any known physical laws or known natural phenomenon that are either explained or yet to be understood by physical laws such as "ball lightning*"* **[4].**

C. Examining the Null Hypothesis:

The object can be explained as either a natural phenomenon of known origin or a misidentified aircraft or aerial phenomenon that can be explained by the physical attributes that it presents for analysis.

The object presents the following seven observable behaviors that appear to be anomalous and must be explained by analysis to confirm the null hypothesis:

1. The object during a 30-minute portion of an infrared heat sensitive FLIR video, RD2 **[2]** travels through the atmosphere flying with no aerodynamic structures for lift that all known aircraft require. This could mean the object is some type of lighter than air object like a weather balloon or large parachute or kite blown by the wind.

2. The object has no visible means of propulsion or heat signature that a reaction or heat engine would produce. It appears to violate the Newtonian laws of motion and thermodynamic conservation of energy **[5].** This could mean the object is some type of lighter than air object like a weather balloon or large parachute or kite blown by the wind.

3. The object appears to be colder than the surrounding environment which eliminates, conventional heat engines, lighter than air aircraft, sail planes or animals such as birds or insects but further analysis reveals that **it may not be colder** than the environment but neither is it hotter as required in item 2 above. Any metallic object such as a Mylar balloon might give a similar appearance of being cold when it is reflecting the temperature of the sky or local environment at higher altitudes. This is an artifact of the sensor technology of the FLIR camera as explained in **Appendix B Sec. 2 (p. 26)**.

4. The object has a fixed structure and appears to rotate, precess or wobble in an aperiodic fashion but returns to fixed orientation multiple times during the video, but the nature of the shape is anomalous and very non-aerodynamic. This might be explained by a collapsed weather balloon that is still partially buoyant and being blown by the wind or perhaps something like a parachute or piece of fabric caught in a high wind. **Appendix D Sec. 1 (p. 34)** gives an analysis of possible structures assuming that the object has a fixed structure and is not some type of plasma phenomenon with no details in its shape.

5. The structure of the object has two parts that seem tethered together by some means such as a very thin cable or line but if so, it appears at times that the background can be seen through the separation of the objects but this may be due to a very thin line that the resolution of the camera's sensor cannot detect. The two parts would tend to give credence to the balloon hypothesis and **Appendix D Sec. 2 (p. 35)** is an examination of the pixel resolution of the object that would prevent small details from being observed.

6. The object has no visible lights or illumination as would be consistent with a conventional aircraft or drone. This would also conform to balloon or wind driven lighter than air object as an explanation.

7. The object is tracked by an airplane and appears to be moving at a velocity against the wind as described one of the pilots in **Appendix F Sec. 6 (p. 46)**. The plane is circling the object at 157 to 245 mph and motion parallax along with the trajectory of the object with respect to the plane may produce a false appearance of high velocity. This is analyzed in **Appendix A Sec. 3-6 (p. 15-25).**

The following arguments against the null hypothesis are based on these seven observables:

1. The null hypothesis would be consistent with some type of balloon, kite or fabric blowing in the wind. In the analysis done in **Appendix A Secs. 2-4 (p.13-21),** assuming that the plane and object are circling the ground at the same average angular velocity, it is possible to calculate the average tangential velocity of the object at different radial distances. In **Appendix B Sec. 4 (p. 28)** a detailed report of weather conditions on the day of the report shows, by weather sounding balloon readings, that the speed of the wind is always lower, at any altitude up to the plane, than the velocity of the object would be at all possible radial distances from the plane at any altitude **[Fig A15 p. 23].**

2. The object gives off no heat signature as would be required by any know means of propulsion but appears cold due to the camera's sensor technology which would record reflected infrared radiation by metallic objects. If the object had some type of engine, then it would display a hotter than the local environment due to either electric propulsion or internal combustion engines and their exhaust.

   Appendix B Sec. 2 (p. 26) explains how the nature of the infrared sensor in the FLIR camera would record the local atmospheric temperature near the balloon or the reflected temperature of the night sky to make the object appear colder than it actually is but only provided if it were a Mylar balloon. Mylar balloons consist of metal (foil) coated plastic such as polyethylene or nylon. Further Mylar balloons are not used for weather balloons as they will break from the pressure differential when rising to an altitude of between 3,000 to 8,000ft **[13].** Latex is used for weather balloon which can rise to 100,000 ft before exploding. Latex is transparent to infrared and would reflect the ground temperature as the camera is looking down from the aircraft. The object cannot be a weather balloon. Further any other object being blown by the wind is slower than the calculated tangential velocity of the object showing it cannot be driven by the wind **[Appendix A Secs. 2-5 (p. 13-23)].**

3. The object appears to have a fixed structure but of a very strange and non-aerodynamic shape that would not present any capability of lift unless it were a lighter than air type of object. See analysis of the shape in **Appendix D Sec. 1 (p. 34).**

4. The rotation of the object violates conventional aerodynamic trajectories except for a balloon, blown by the wind, with some type of attachment. The shape is similar to a partially deflated balloon being observed from above but its heat signature is not consistent with this observation as mentioned above. It appears to be more rigid and not consistent with a wind driven balloon as it circles in a fairly consistent manner and not with the randomness one would expect from a wind driven object **[7]** and **Appendix D Sec. 1 (p. 34).**

5. Wind speeds as shown in **Appendix B Sec. 4 (p. 28)** are in the 3-45 mph range but calculations of the **co-radial tangential velocity Vt_o** at all altitudes **[Appendix A Sec. 5 (p. 22)]** rule out this as being a balloon because the wind speeds are too low at all altitudes from ground level up to the plane. Topography maps of the area indicate that it flies over mountains that are 3,750 feet in height and the object appears to be above the terrain at all times.

6. If the object were a small piece of paper or fabric composed of two sections attached by a thin strip and close to the airplane it would not be able to keep up with the speed of the aircraft. The high magnification factor of narrow FOV **[Appendix C #14 (p. 33)],** would be able to see the details of this close object.

7. The object has no lights and has a long endurance which would rule out most quad-copter type of drones although some specialty drones can achieve several hours of flight time with large batteries or hybrid gas electric systems **[17]** but these have characteristic shapes. Other long endurance drones have wings like airplanes. In our analysis its shape is not consistent with any known powered drone **[Appendix D Sec. 2 (p. 35)].**

The arguments in favor of the null hypothesis include:

1. This may be some unknown type of natural phenomenon like an atmospheric plasma form that is currently poorly understood.

2. The object may be a revolutionary type of vertical lift drone, but since it has no lights or visible engines with a heat signature, it would have to be some unknown or secret device operating in a dangerous manner outside the aviation rules of the United States that would endanger aircraft. This would require further research as it presents a danger to aircraft safety and may be a foreign asset that threatens national security.

D. Uncertainties and Error Bounds:

1. Wind speed calculations were taken from weather sounding data in Tucson, Arizona about 65 miles away from the observation but similar readings were taken at Flagstaff, Arizona 306 miles away **[16]** and Santa Teresa, New Mexico 372 miles away **[15]** showing little difference in regional wind speed at the time of the observations **[Appendix B Sec. 4, 5 (p. 28), Fig B3 and B4].** Estimated standard deviation of error ± 10%. Three standard deviations were used to arrive at a confidence level of 99.73%
2. Co-radial Tangential velocity error bounds were calculated with a standard deviation of % error of 7.09% **[Appendix A, Figs. A11** and **A12 (p. 21)]** three standard deviations were used to arrive at a confidence level of 99.73% for the comparison to wind speed.
3. Size estimations of the object, with an error estimated at 8.7% **[Appendix D, Sec. 2, Fig. D3 (p. 36)]** due to pixel resolution, ranged between 1ft to 9 ft due to the uncertainty of the object's altitude and distance from the plane **[Appendix A Sec. 6 (p. 24), Fig A16**; **Appendix D Sec. 2 Figs D3, D5** and **D6, (p. 36-39)]**

E. Conclusion:

The author of this report concludes that the arguments against the null hypothesis far outweigh the arguments in support of the null hypothesis. This supports the conclusion that the object cannot be explained by any known natural phenomenon or technology that is used for aeronautical propulsion.

The report derives the kinematic characteristics of the object **[Appendix A Secs. 2-4, (p.13-21)]** with error bounds on its size and its tangential velocity at different assumed altitudes. It also explains and refutes the apparent indication that it is colder than the surrounding environment **[Appendix B Sec. 2**

(p. 26)] due to an artifact of how the FLIR image sensor functions. It describes the geographical trajectory of the object during the RD2 video **[Appendix E Sec. 1,2 (p. 40-43)].**

F. Discussion

The author concludes the object is anomalous and worthy of scientific investigation. The motivation behind the investigation of this object is to convince the scientific community that there are phenomena in the atmosphere that appear to be solid objects flying with characteristics that appear to defy the current understanding of physics: Congress after receiving many reports of these mysterious objects as recently reported in the disclosures by the United States Navy **[19]** Statement by the Department of Defense on the release of historical Navy videos April 27, 2020 which led to a congressional bill by Senators Gillebrand, Rubio and Galegos **[20]** has mandated that a serious study to understand the nature of these objects must be undertaken by the Department of Defense and reported to Congress. This resulted in the Office of the Director of National Intelligence's report "Preliminary Assessment: Unidentified Aerial Phenomena", 25 June 2021 **[18],** and from p.4-5

> "...144 reports originated from USG sources. Of these, 80 reports involved observation with multiple sensors. Most reports described UAP as objects that interrupted pre-planned training or other military activity...In 18 incidents, described in 21 reports, observers reported unusual UAP movement patterns or flight characteristics. Some UAP appeared to remain stationary in winds aloft, move against the wind, maneuver abruptly, or move at considerable speed, without discernible means of propulsion. In a small number of cases, military aircraft systems processed radio frequency (RF) energy associated with UAP sightings."

These reports have been reported by both military, Navy and Air Force personnel and have a long history of over 70 years of infrequent reports of extraordinary phenomenon. These objects are of a nature, that like meteorites, are not repeatable but are worthy of study because they may lead to a better understanding of physics or reveal some new information of reality that falls within the established goals of physical science. The UAP phenomena is varied and complex.

G. Recommendations for Further Scientific Study:

The study of UAP will require a substantial investment in specialized equipment placed at multiple locations and require major investments in time and money to understand their nature. The model that science uses to investigate meteors with cameras and telescopes or earthquakes, using geological seismic earthquake wave monitoring stations, which are also events that do not repeat but have finally been understood, is appropriate for this phenomenon. These stations should be equipped with sensors that can take photographic and video recordings in optical and infrared frequencies and measure other forms of RF radiation, ionizing radiation, gravitational disturbances and other data to begin to understand the underlying physics they present. These objects may be a hazard to aerial transportation and be a dangerous distraction to pilots in certain situations. The author as a member of the SCU hopes this paper will be a small step to move the scientific community in that direction.

Acknowledgements:

Contributors and Reviewers: David Falch, Robert Powell, Chahé Adourian, Dr. Patrick Koehn

References:

[1] https://www.youtube.com/watch?v=mNCgDjoucRM

[2] https://zenodo.org/record/7301342/files/Rubber Duck 2.ts?download=1

[3] https://www.investopedia.com/terms/n/null_hypothesis.asp

[4] https://en.wikipedia.org/wiki/Ball_lightning

[5] https://en.wikipedia.org/wiki/Heat_engine

[6] https://www.flir.com/products/star-safire-380-hd/

[7] https://zenodo.org/record/7301342/files/Final FLIR Video Showing False Heat Indications.mp4?download=1

[8] https://en-us.topographic-map.com/maps/nrsb/Buenos-Aires-National-Wildlife-Refuge/

[9] https://www.layertec.de/en/capabilities/coatings/metallic

[10] https://maps.co/gis/

[11] https://www.ncei.noaa.gov/products/climate-data-records

[12] https://en.wikipedia.org/wiki/Nyquist%E2%80%93Shannon_sampling_theorem

[13] https://www.sanluisobispo.com/news/weather/weather-watch/article39489087.html

[14] https://en.wikipedia.org/wiki/Image_scaling

[15] Santa Teresa New Mexico Weather Sounding Data November 23, 2019 12:00Z

[16] Flagstaff Arizona Weather Sounding Data Nov 23, 2019 12:00Z

[17] https://botlink.com/blog/the-3-main-categories-of-drones-and-their-advantages-and-disadvantages

[18] https://www.dni.gov/files/ODNI/documents/assessments/Prelimary-Assessment-UAP-20210625.pdf

[19] Statement by the Department of Defense on the Release of Historical Navy Videos April 27, 2020

[20] December 09, 2021Gillibrand's Groundbreaking Unidentified Aerial Phenomena Amendment

[21] https://www.researchgate.net/publication/268357096

[22] https://en.wikipedia.org/wiki/Normal_distribution#Operations_on_two_independent_normal_variables

Return to top

Appendix A: Kinematic and error bound analysis of the object from the RD2 video

1. Overview: In the following analysis the author will derive the size, altitude and speed of the object by using the known parameters of the camera and the meta data reading of the FLIR (Forward Looking Infrared Camera) **[6]** presented to a screen that the pilot views as he scans the ground below. Throughout the portion of the video that is analyzed the field of view of the camera α, visible in the metadata as **narrow** is α = 1.3° **[Appendix C item 10 (p. 32)]** which makes the camera have a high telescopic capability.

The metadata presented on the screen is quite varied but for our purposes there are two important angles to where the camera is pointing. These angles are constantly changing as the camera operator manually tracks the object keeping it approximately centered on the screen. The angle β, is the angle that the camera points down from the horizontal axis of the airplane. This is not locked to the angle of the plane with respect to the ground, but to the nose of the aircraft, as this is available to the pilot but is not available to the camera. More discussion about this will be presented later in this document.

The other angle γ is the azimuth angle of the camera which is defined as 0°or 360° pointing straight ahead of the plane, 90° rotating right clockwise from the nose of the plane, 180° clockwise pointing directly behind the plane and 270° clockwise pointing left of the direction of the plane. Again, these are with respect to the longitudinal axis of the airplane or in other terms the direction of the plane flying forward and are not related to geographical coordinates as these are unknown to the camera. See Figure A1.

The altitude of the plane is A and the object's altitude and distance from the plane is unknown. The figure A1 shows the object at three different altitudes from the ground level, h1, h2 and h3. The distance from the plane's altitude and the altitude of the plane above the objects different positions are shown as A-h1, A-h2 and A-h3. The object's diagonal distance from the cameras sensor and the three positions are Sdd1, Sdd2 and Sdd3 and are calculated from the cosine relationship between 90-β degrees and the vertical distance between the plane's height and the object's height above ground A-h1, A-h2 and A-h3. The figure only shows 3 positions but the calculations are done for 20 (every 90 sec) and 80 (every 22.5 sec) equal time increments throughout the video to overcome possible Nyquist Sampling rate errors **[12]** due to under sampling the highest frequency components of the velocity in the video. It shows that 20 samplings give the same result as 80 sampling points for the average velocity indicating no under sampling errors are occurring. Figure A1 shows a 3-dimensional coordinate system with X and Y being the ground level coordinates and Z being the altitude above ground.

Throughout the video **[2]** the object is clearly below the airplane and the horizon is not visible so the angle β is never 0° **[Fig A17 (p. 25)]** and is always negative over a range of -39° as will be discussed later. During the entire time of the analysis the altitude of the plane remains nearly constant deviating by approximately ± 15 ft **[Fig A6, Column 3 (p. 16)]** but the plane is dipping and banking as it tracks the object through an approximate 25 square mile area **[Fig A8 (p. 17)]** position on the ground. This introduces an uncertainty in β as some of the variation is due to the plane banking and dipping or the object changing altitude as the plane circles the circling object. So, some of the β is due to the dipping

of the plane and some due to the object changing altitude and more discussion will be presented later on how this is treated in the analysis **[Fig A17 (p. 25)].**

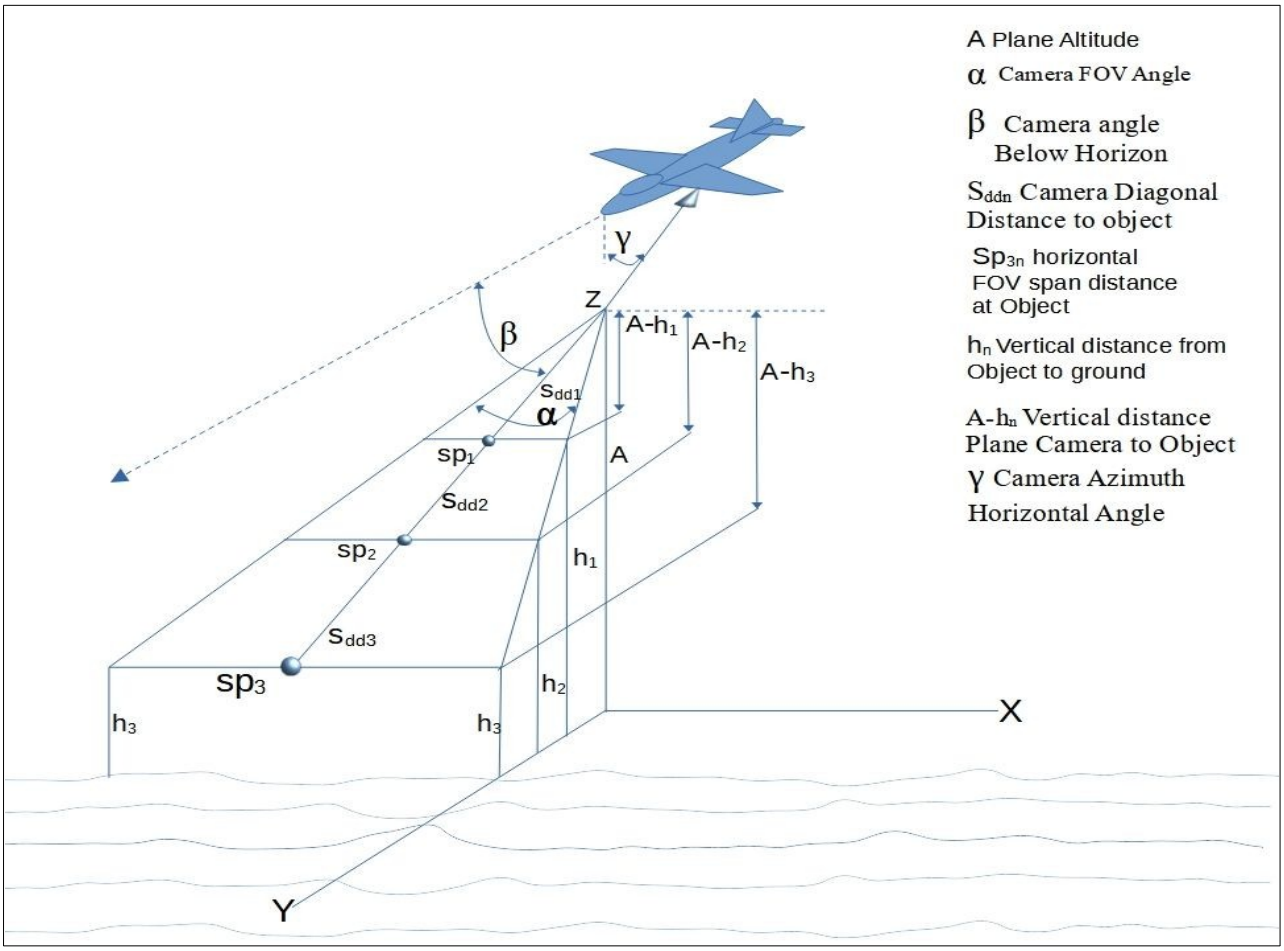

Figure A1: Trigonometric definitions used in the kinematic analysis

Figure A1 shows the calculation relationships to derive the different span diagonal (Sddn) distances. The span is the linear distance spanned by the cameras field of view (FOV) that is shown on the video screen for horizontal distance on the screen. The horizontal distance on the screen corresponds to physical distance spans of Sp1, Sp2 and Sp3 which increases in value the farther away from the plane. Twenty values are calculated and will be used to derive the size and velocity of the object based on its altitude and span distance from the plane. This will give the possible values of the object's kinematics that will be tested against the observed anomalies and the null hypothesis.

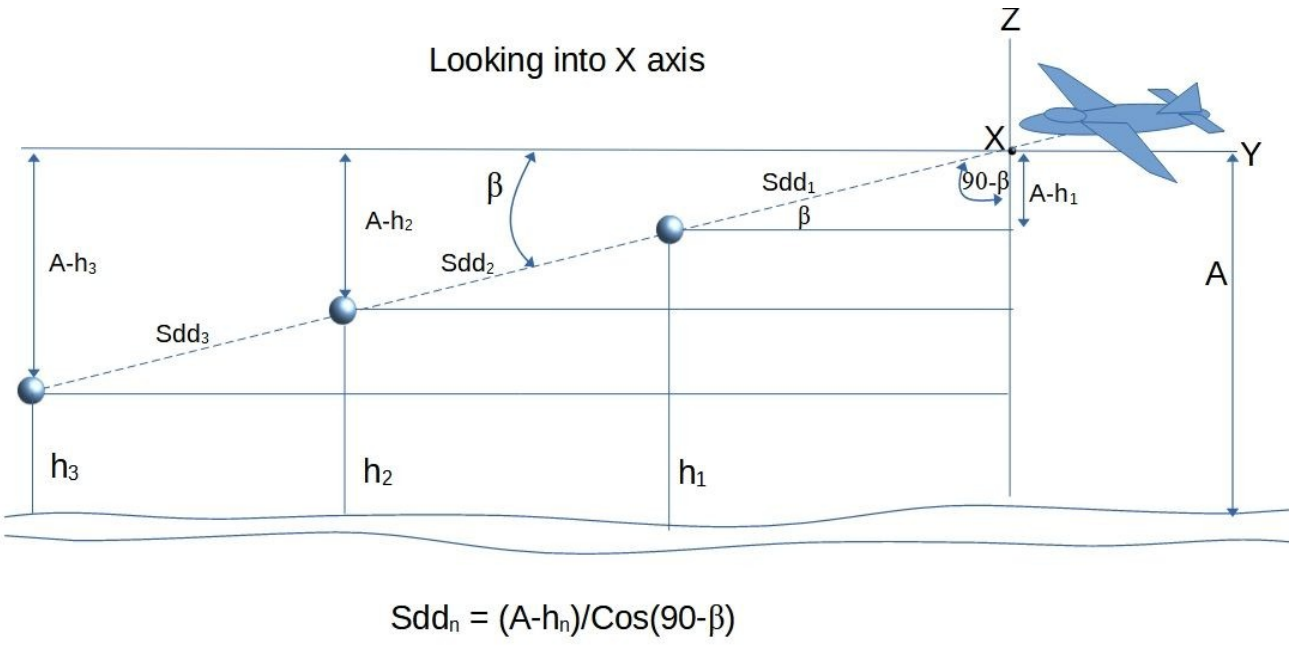

Figure A2: Derivation of the Span Diagonal Distance relationship

Figure A2 is a view looking into the X axis or side view of the plane with the camera pointing down β degrees and the angle 90-β is used for the right triangle formed by Sddn and A-hn where the cosine of 90-β degees is defined as (A-hn)/Sddn and when solved for Sddn = (A-hn)/Cos(90-β) as shown in figure A2. This relationship is used to calculate 20 values of Sddn for n= 1 to 20 and a table is derived for distance between the plane and object and its span diagonal distance to the object for the 20 positions. We formalize this for later analysis:

$$Sddn = \frac{(A - hn)}{(\cos(90 - \beta))} \qquad \text{E1}$$

and

$$hn = A - Sddn * \cos(90 - \beta) \qquad \text{E2a}$$

$$dhn = Sddn * \cos(\beta) \qquad \text{E2b}$$

Figure A3 is a view looking into the Z axis or looking down on the plane from above. It uses the field of view of the camera's lens to calculate the span distance for each of the span diagonal distances calculated in Figure A2 above.

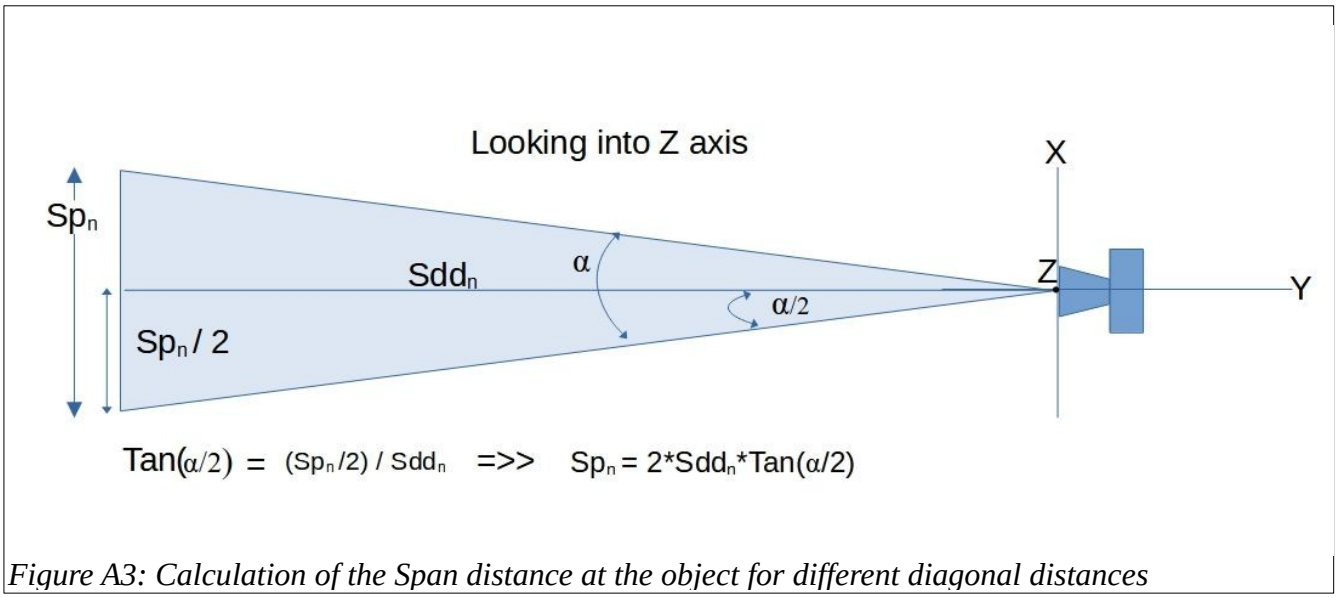

Figure A3: Calculation of the Span distance at the object for different diagonal distances

Figure A3 shows how the span distance is derived from the trigonometric tangent relationship where a right triangle is formed by the angle α/2 and the half the span distance Spn/2 so by definition of the tangent, Tan(α/2) = (Spn/2)/Sddn and solving for Spn we get Spn = 2*Sddn*Tan(α/2). This is added to the table of calculations for the 20 values of Sddn.

$$Spn = 2 * Sddn * \tan\left(\frac{\alpha}{2}\right) \qquad \text{E3}$$

2. Calculation of the velocity in the Horizontal direction shown on the FLIR screen:
As observed in the RD videos **[1], [2]** the object moves from right to left as the plane tracks it. It also moves somewhat in the vertical direction but there is little overall change in altitude and this velocity is assumed to be zero as it not necessary for this analysis.

It is at first glance difficult to determine the speed of the object as both the object is moving as well as the plane and the pointing angles of the camera, as the camera operator manually tracks the object. After some consideration, if we imagine that the object is stationary then it would move off the screen as the plane moves to the left. Since the object stays approximately stationary on the screen, with the plane falling behind slowly or moving ahead faster, as the camera operator tries to keep the object centered, we can reduce the object's velocity $V_o(t)$ to its vector components of Vt_o tangential velocity parallel to the plane (this is what is projected on the camera's screen) and Vt_n the normal velocity to the plane that add up to form $V_o(t)$, the object's velocity, as long as the camera operator keeps the object approximately locked to the screen. This gives a velocity estimate of object if it stays on the screen to within about $\pm$ 7.09% standard deviation **[Fig A11 (p. 21].** This is shown in figure A4 below. The field of view intersects the object and is recorded on the FLIR sensor which it converted to an image on the screen. There is an error introduced when the object is not perfectly parallel to the plane as shown in Figure A4 as error angles $\pm \boldsymbol{\gamma_\varepsilon}$ which will be used for an error analysis.

The vector components of the Object's velocity $V_o(t)$ are from the right triangle formed by 90 γ' in figure A4 for error angles $\pm \gamma_\varepsilon$, note when near the plane and γ' = 90°, Vto = Vp which is the co-radial component that falls off in velocity as the distance increases away from the plane. See **Fig A10 (p. 20)**.

$$Vto = Vto_{+\varepsilon} * \cos([90 - \gamma']^\circ) \text{ and } Vto = Vto_{-\varepsilon} * \cos([\gamma' - 90]^\circ) \qquad \text{E4}$$

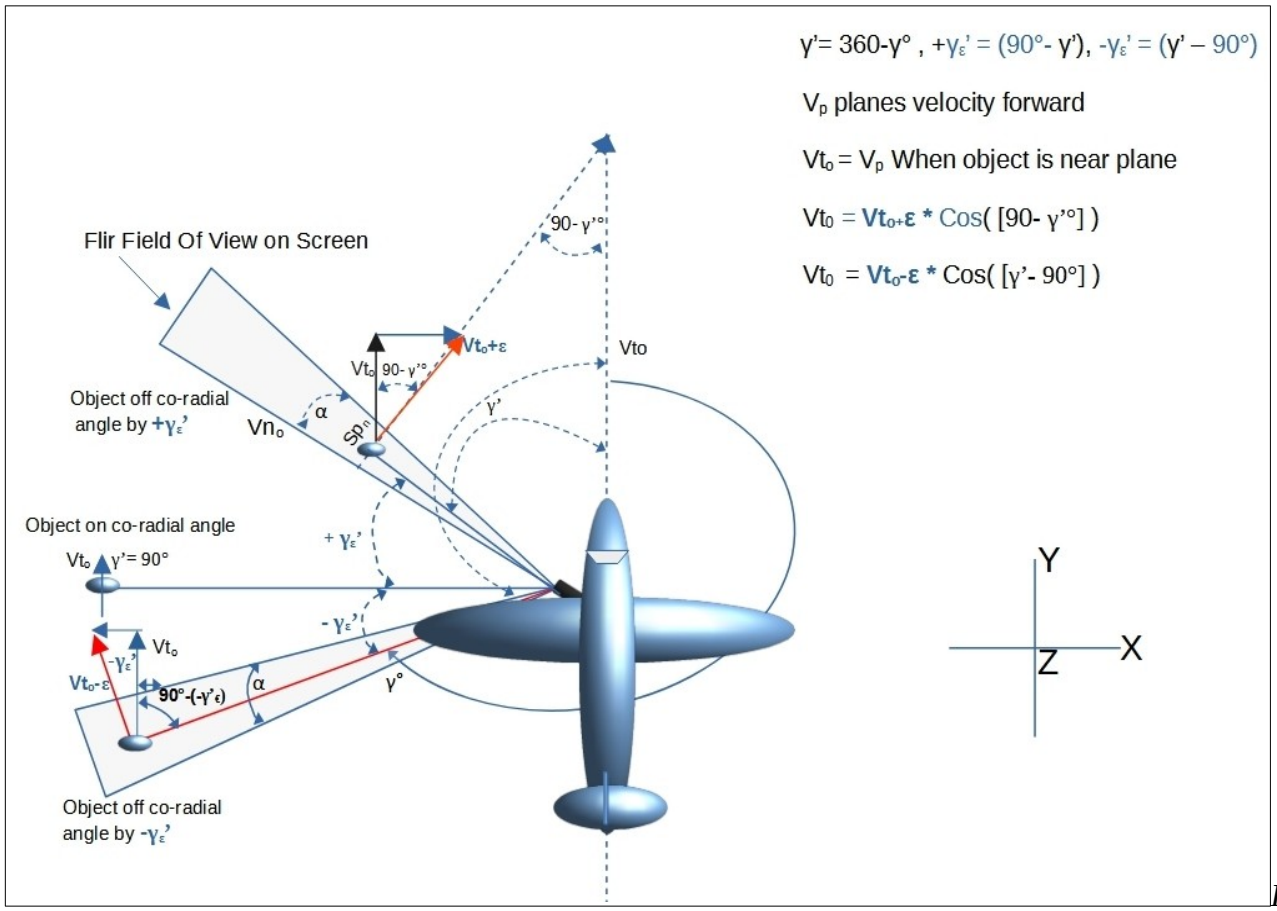

Figure A4: Calculation of objects velocity assuming tracking is locked on screen Looking into Z axis

We start assuming the object is near to the plane at the same altitude (β = 0°) as the plane but with some thought we see that the projection of this triangle is true for any height of the object where Vn and Vp are the projection of the velocity vector's triangle at the height of the object for different β angles. From figure A4 if γ'= 90° the object would be moving parallel to the plane, the author defines this as a co-radial trajectory that will be discussed in detail later. It will then have the tangential γ velocity Vt = Vp, the same as the plane but if it is at less of an angle, then its velocity is smaller until γ' = 0°, where its tangential velocity Vt would be 0 and its Normal Velocity would be Vp relative to the plane's shadow at the height of the object. The conversion of γ' = 360°- γ is convenient because the camera records this angle clockwise but the calculation is done for the small triangle angular measurement.

3. Data Base used for the Calculations of average values for Vp, γ and β:
The RD2 video was sampled at 2-minute intervals to produce the source data to calculate the size and velocity of the object. The source data table is shown in **Fig A8 (p. 17).** To guarantee that the planes velocity Vp was not under sampled according to the Nyquist / Shannon Sampling rate [12]. The

Minutes	Seconds	Plane Velocity Vp Knts	Altitude ft	β Angle down degrees	γ Side angle Degrees	Plane Speed Vp Mph	Minutes	Seconds	Plane Velocity Vp Knts	Altitude ft	β Angle down degrees	γ Side angle Degrees	Plane Speed Vp Mph
0.00	22.50	172.00	14800.00	-12.00	256.00	197.80	15.00	22.50	189.00	14803.00	-40.00	232.00	217.35
0.00	45.00	169.00	14791.00	-11.00	281.00	194.35	15.00	45.00	201.00	14803.00	-18.00	224.00	231.15
1.00	7.50	186.00	14804.00	-31.00	288.00	213.90	16.00	7.50	213.00	14802.00	-2.00	241.00	244.95
1.00	30.00	204.00	14805.00	-31.00	264.00	234.60	16.00	30.00	210.00	14803.00	3.00	272.00	241.50
1.00	52.50	215.00	14804.00	-18.00	247.00	247.25	16.00	52.50	193.00	14803.00	-5.00	292.00	221.95
2.00	15.00	203.00	14803.00	-5.00	262.00	233.45	17.00	15.00	182.00	14805.00	-24.00	299.00	209.30
2.00	37.50	177.00	14801.00	-8.00	285.00	203.55	17.00	37.50	182.00	14806.00	-21.00	277.00	209.30
3.00	0.00	167.00	14804.00	-33.00	280.00	192.05	18.00	0.00	171.00	14796.00	-12.00	283.00	196.65
3.00	22.50	166.00	14801.00	-29.00	253.00	190.90	18.00	22.50	165.00	14801.00	-16.00	291.00	189.75
3.00	45.00	162.00	14782.00	-4.00	270.00	186.30	18.00	45.00	166.00	14803.00	-34.00	288.00	190.90
4.00	7.50	175.00	14801.00	-33.00	286.00	201.25	19.00	7.50	167.00	14807.00	-35.00	250.00	192.05
4.00	30.00	177.00	14804.00	-27.00	249.00	203.55	19.00	30.00	170.00	14800.00	-19.00	237.00	195.50
4.00	52.50	199.00	14791.00	-6.00	258.00	228.85	19.00	52.50	180.00	14800.00	-7.00	242.00	207.00
5.00	15.00	212.00	14804.00	-7.00	273.00	243.80	20.00	15.00	200.00	14800.00	2.00	264.00	230.00
5.00	37.50	211.00	14809.00	-27.00	265.00	242.65	20.00	37.50	214.00	14809.00	-13.00	283.00	246.10
6.00	0.00	199.00	14802.00	-4.00	274.00	228.85	21.00	0.00	216.00	14809.00	-14.00	278.00	248.40
6.00	22.50	174.00	14800.00	-26.00	296.00	200.10	21.00	22.50	211.00	14805.00	-13.00	277.00	242.65
6.00	45.00	174.00	14802.00	-31.00	268.00	200.10	21.00	45.00	199.00	14804.00	-13.00	279.00	228.85
7.00	7.50	163.00	14783.00	-11.00	283.00	187.45	22.00	7.50	183.00	14804.00	-11.00	282.00	210.45
7.00	30.00	162.00	14804.00	-35.00	260.00	186.30	22.00	30.00	171.00	14802.00	-21.00	281.00	196.65
7.00	52.50	165.00	14798.00	-5.00	252.00	189.75	22.00	52.50	166.00	14801.00	-21.00	274.00	190.90
8.00	15.00	186.00	14794.00	-7.00	277.00	213.90	23.00	15.00	166.00	14801.00	-21.00	268.00	190.90
8.00	37.50	196.00	14803.00	-33.00	255.00	225.40	23.00	37.50	169.00	14800.00	-20.00	260.00	194.35
9.00	0.00	210.00	14793.00	-5.00	261.00	241.50	24.00	0.00	178.00	14800.00	-16.00	253.00	204.70
9.00	22.50	210.00	14800.00	-6.00	280.00	241.50	24.00	22.50	190.00	14801.00	-14.00	251.00	218.50
9.00	45.00	204.00	14806.00	-28.00	266.00	234.60	24.00	45.00	202.00	14804.00	-11.00	250.00	232.30
10.00	7.50	188.00	14795.00	-3.00	276.00	216.20	25.00	7.50	213.00	14804.00	-12.00	257.00	244.95
10.00	30.00	167.00	14798.00	-29.00	297.00	192.05	25.00	30.00	216.00	14811.00	2.00	258.00	248.40
10.00	52.50	166.00	14799.00	-18.00	273.00	190.90	25.00	52.50	210.00	14814.00	-5.00	277.00	241.50
11.00	15.00	164.00	14798.00	-32.00	260.00	188.60	26.00	15.00	197.00	14814.00	-7.00	291.00	226.55
11.00	37.50	167.00	14789.00	-5.00	264.00	192.05	26.00	37.50	188.00	14817.00	-22.00	290.00	216.20
12.00	0.00	187.00	14800.00	-33.00	276.00	215.05	27.00	0.00	188.00	14814.00	-13.00	271.00	216.20
12.00	22.50	196.00	14806.00	-10.00	255.00	225.40	27.00	22.50	174.00	14804.00	-10.00	281.00	200.10
12.00	45.00	213.00	14804.00	-8.00	269.00	244.95	27.00	45.00	167.00	14804.00	-15.00	282.00	192.05
13.00	7.50	206.00	14811.00	-11.00	282.00	236.90	28.00	7.50	166.00	14798.00	-17.00	280.00	190.90
13.00	30.00	187.00	14808.00	-25.00	287.00	215.05	28.00	30.00	168.00	14800.00	-19.00	276.00	193.20
13.00	52.50	184.00	14806.00	-23.00	256.00	211.60	28.00	52.50	174.00	14801.00	-20.00	268.00	200.10
14.00	15.00	166.00	14804.00	-6.00	273.00	190.90	29.00	15.00	182.00	14802.00	-21.00	257.00	209.30
14.00	37.50	166.00	14801.00	-21.00	294.00	190.90	29.00	37.50	192.00	14801.00	-15.00	247.00	220.80
15.00	0.00	178.00	14803.00	-40.00	281.00	204.70	30.00	0.00	203.00	14800.00	-9.00	247.00	233.45

Samples Taken	Plane Velocity Vp Knts	Altitude ft	β Angle down degrees	γ Side angle Degrees	Plane Speed Vp Mph	Object's Vt Velocity Mph	Object's Vn Velocity Mph
20 Samples Taken	183.35	14799.75	-19.45	269.90	210.85	204.98	42.08
40 Samples Taken	185.30	14800.80	-17.40	271.70	213.10	207.98	39.34
60 Samples Taken	189.15	14803.25	-15.65	268.60	217.52	202.09	66.93
80 Samples Taken	185.45	14804.55	-14.30	266.90	213.27	206.60	46.11
80 Samples Average	185.81	14802.09	-16.70	269.28	213.68	205.41	48.62

Minutes	Seconds	Plane Velocity Vp Knts	Altitude ft	β Angle down degrees	γ Side angle Degrees	Plane Speed Vp Mph

Average of 17 samples of planes velocity Vp taken every 2 minutes is 213.70 Mph which is very close to the 80 sample average of 213.68 Mph taken every 22.5 seconds. This indicates that the sampling rate is not under sampled and meets the Nyquist rate.

Figure A5: 80 samples of the planes velocity Vp taken every 22.5 sec throughout the Rd2 video to show that the sampling meets the Nyquist rate and is not an under sampled average value of Vp

velocity the video was resampled 80 times shown in Figure A5 to compare the average calculated values. The values are virtually identical indicating that the average value of Vp is about 213.70 mph.

RD2 2 Minute Interval Data Base					
Time [Min . Sec]	**Plane Speed Knts**	**Altitude ft**	**β Angle down degrees**	**γ Side angle Degrees**	**Vp Plane Speed Mph**
0.34	166.00	14,794.00	-6	269	190.90
1.34	207.00	14,804.00	-30	258	238.05
3.34	162.00	14,786.00	-5	254	186.30
5.34	211.00	14,804.00	-25	270	242.65
7.34	162.00	14,803.00	-34	250	186.30
9.34	204.00	14,804.00	-29	282	234.60
11.34	165.00	14,794.00	-5	260	189.75
13.34	185.00	14,810.00	-34	286	212.75
15.34	194.00	14,803.00	-25	224	223.10
17.34	182.00	14,805.00	-25	288	209.30
19.34	172.00	14,799.00	-16	237	197.80
21.34	205.00	14,806.00	-13	278	235.75
23.34	168.00	14,800.00	-20	261	193.20
25.34	216.00	14,816.00	5	264	248.40
27.34	170.00	14,806.00	-15	282	195.50
29.34	190.00	14,801.00	-16	248	218.50
30.00	200.00	14,801.00	-10	246	230.00
AVG	185.82	14,802.12	-17.82	262.18	213.70

Figure A6: 30min at 2 min interval Samples of the Planes Velocity from RD Video as source data it varies approximately ± 15ft in altitude over the sampling period.

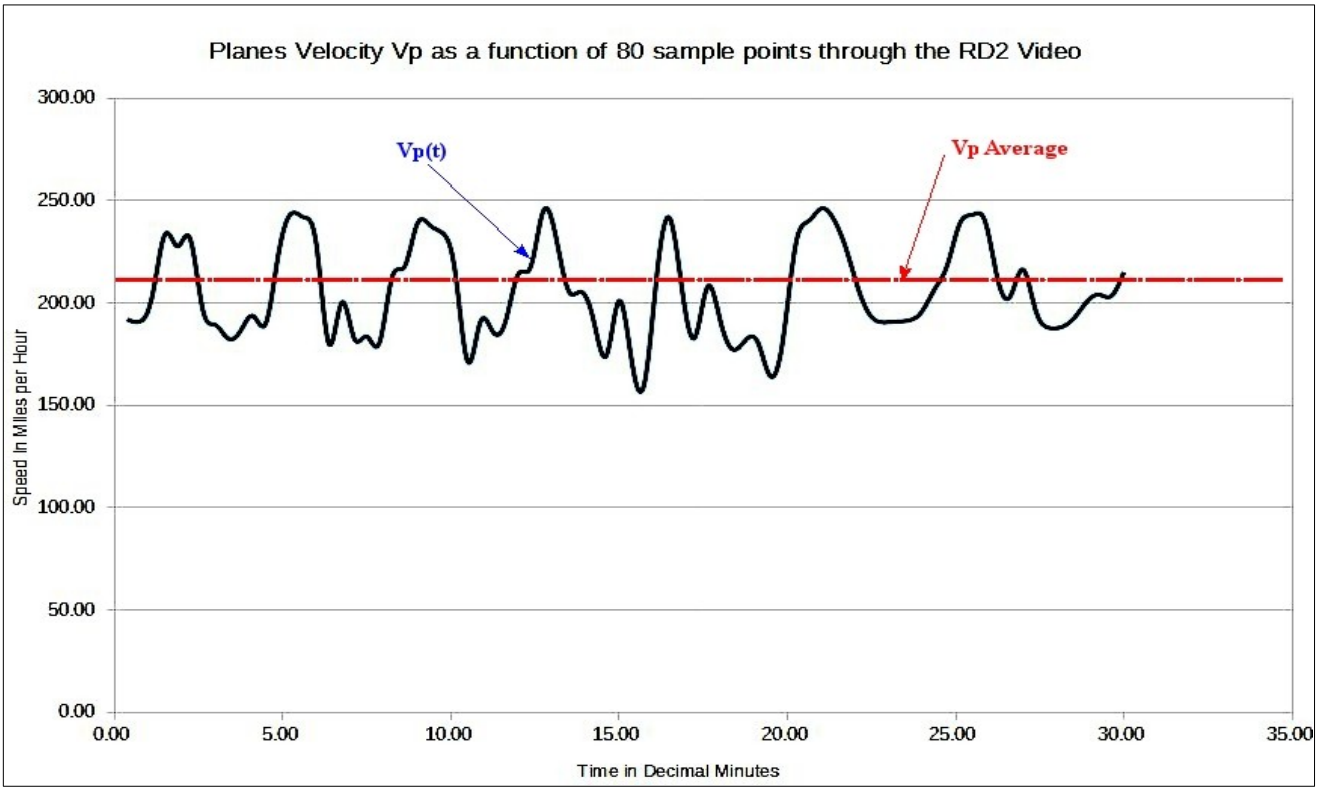

Figure A7: This shows the instantaneous velocity Vp(t) is both greater or less then than the average velocity. This allows for an analytical analysis as shown in equation E6 and figure A9

4. Calculating the tangential velocity with motion parallax taken into consideration

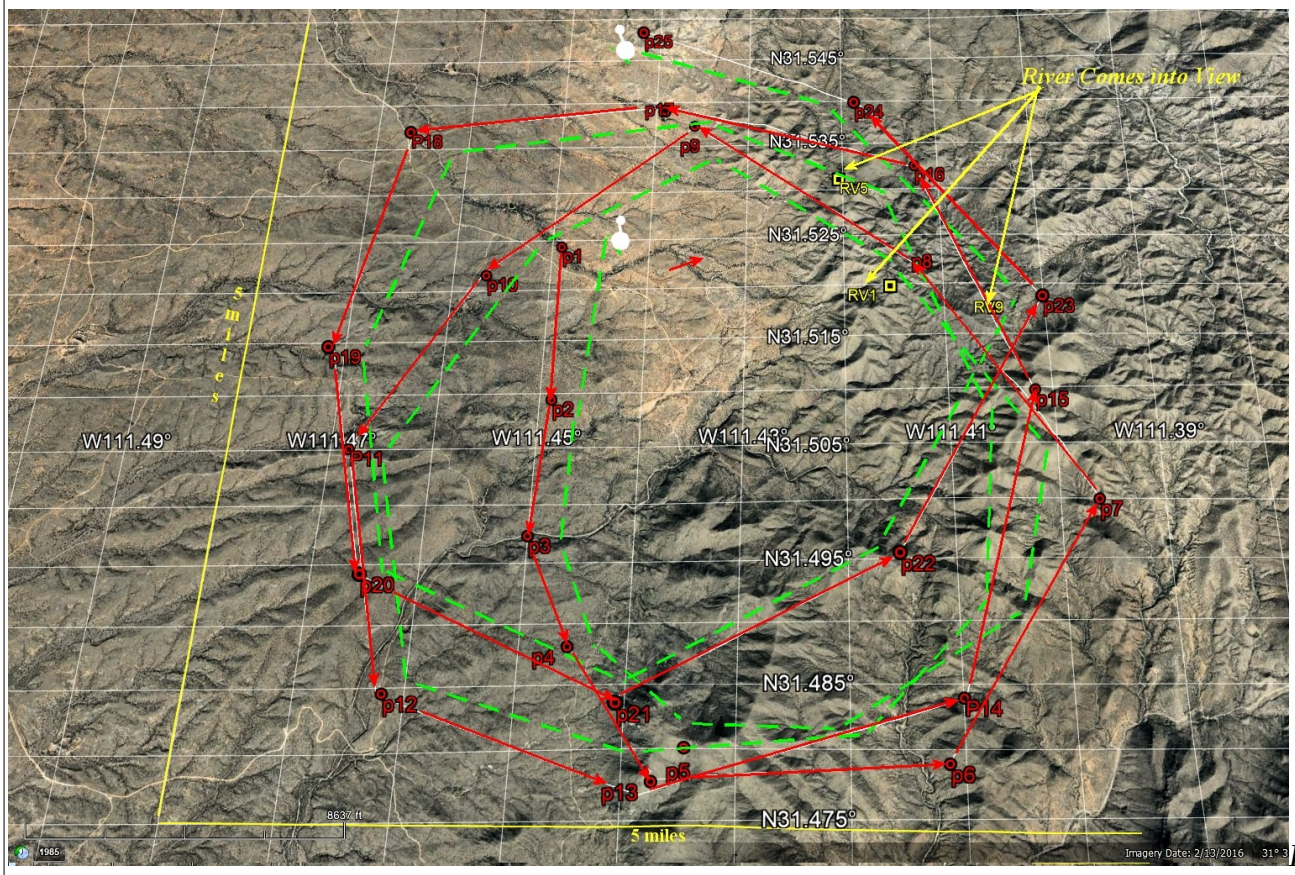

Figure A8: The planes trajectory in red P1-P25, from the FLIR's metadata [Appendix C, item2, p32] for 3 rotations about the ground as it follows the object around an approximate 25 square mile area. Green path is hypothetical path of object kept in sight by the plane with same angular acceleration. The Yellow points RV1, RV5 and RV9 show a river that comes in and out of view as the object passes it, indicating that the object is not stationary or circling in a short radius about the ground. The tangential velocity of the rotating object is calculated for different distance from the plane based on the angle γ and different possible altitudes for the object.

Figure A8 shows the trajectory of the plane for the first 3 circular transits around the ground following the object in the RD2 video. This was taken from the first 25 of sampling points, every 22.5 sec in the video. As the objects moves through the video from left to right there are no repeating or quasi-stationary objects in the landscape as would be the case, if the object was stationary or moving in a very short circular trajectory. When the background is observed it is noted that a river comes into view every few minutes as the plane and object pass over the river but most of the time the background does not repeat or have any landmarks that remain the same. Since the object is being manually tracked by the FLIR camera operator it remains approximately centered on the screen and so the average angular velocity of the object matches that of the plane. The river comes into view at RV1, RV5 and RV9 which on the terrain map, shown in yellow, are located in similar positions indicting it is the same river coming into and out of view as the plane circles different trajectories.

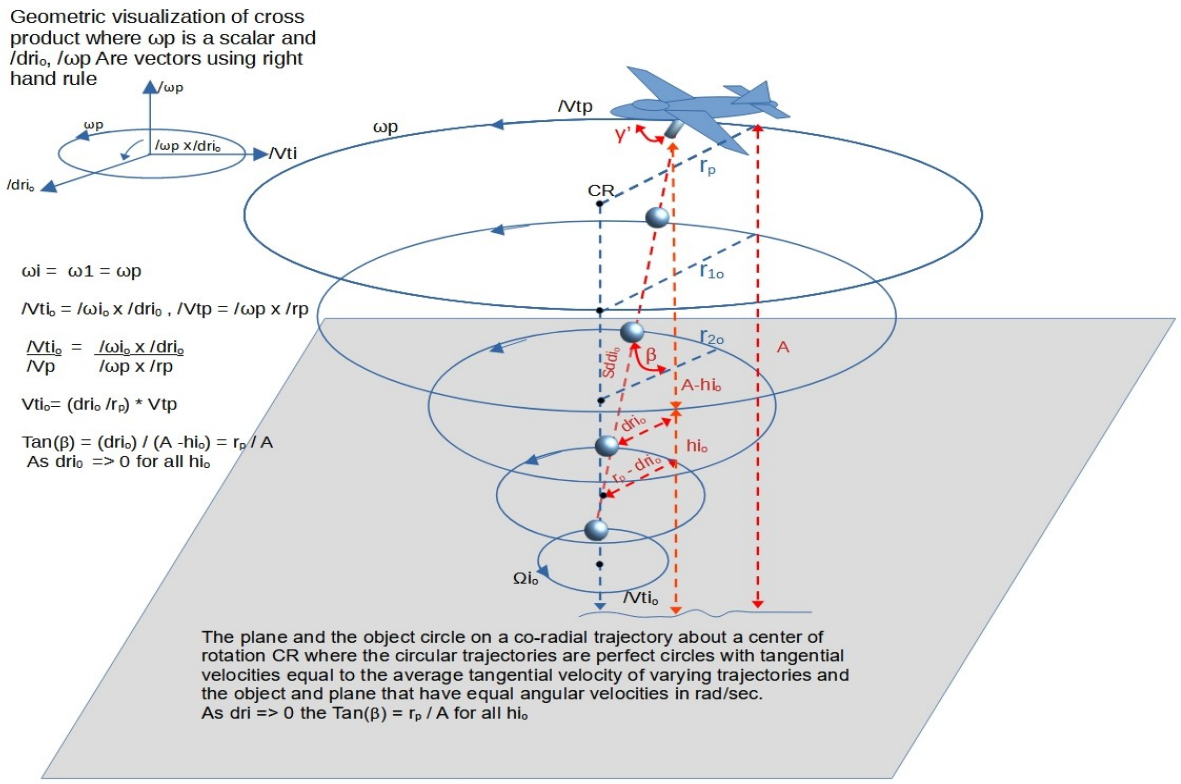

*Figure A9: shows the plane circling with the object at the edge of the cone, the object is at an unknown vertical distance A-hi$_o$ from the camera and radius dri$_o$ or horizontal distance from the CR. Since the object has the same average angular velocity as the plane, at any altitude, it is possible to calculate the co-radial tangential velocity Vt$_o$ from the relationship between dri$_o$ = (A-hi$_o$)*Tan(β) and A - hi$_o$ due to similar triangles of angle Beta. This provides a convenient way to calculate the tangential velocity of the object Vt$_o$ as a proportion of Vp, the planes velocity as it circles the object. We are assuming an approximate circular velocity so that we can calculate a tangential velocity that the object will be traveling at on average. This is used to compare to the local wind velocity at different altitudes to see if it is possible that object is being propelled by the wind or by some other means.*

Figure A9 and A4 show diagrams of the geometry involved in determining the co-radial tangential velocity of the object for various altitudes and distances from the camera. First the angular velocity of the plane on average is the same for the plane and the object so we can write: ωi$_o$ = ω1 = ωp or the angular velocity of the plane is the same for any altitude as that of the object. From basic physics we can write that the tangential velocity of the rotating object is the vector cross product of the radius of rotation r, (dri$_o$ in our case) and the angular velocity ωi$_o$ or in the general case, /$\underline{Vt_o}$ = /$\underline{\omega_o}$ x /$\underline{r_o}$ and since we are only interested in the scalar components of the velocity $Vt = \omega * r$ so by inspection we can see that for our figure A9

$$\omega p = \frac{Vti_o}{dri_o} = \frac{Vp}{r_p} = \frac{Vt_1}{dr_1} \qquad \textbf{E5}$$

From E5 by solving for Vti where dh is the radius of the plane at altitude A as it circles the object over the ground and since $\omega i_o = \omega 1 = \omega p$

Further $\tan(\beta) = \frac{dri_o}{(A - hi_o)} = \frac{r_p}{A}$ as $dri_o \Rightarrow 0$ for all β so since hi is assumed and A is known we can calculate Vti, the tangential velocity of the object at any radius dri, which is just the ratio of the object's radius to the plane's radius about CR times the planes velocity shown in E6. From E5 by solving for Vti where r is the radius of the plane at altitude A as it circles the object over the ground and since $\omega i_o = \omega 1 = \omega p$, it is not necessary to know r_p, just the ratio of dri_o to r_p .

$$Vti_o = \left(\frac{dri_o}{r_p}\right) * Vp \qquad \textbf{E6}$$

Figure A10: Shows the co-radial trajectory of the plane, *A – hi,* above the object and *dhi* horizontally from the object, from a perspective looking down on the plane and the object, as it tracks the object circling some location on the ground both in blue. In red is the average circular trajectory of the plane and object at different altitudes, only one of many altitudes hi, is shown for the object in blue, for simplicity. We can see that due to the narrow field of view of the FLIR camera which is only 1.3° that if the object was out of the field of view at any other position but P1 it would not be seen on the screen. We know from the meta data that the plane is circling a location on the ground as previously shown in Figure A8 and since it is keeping the object centered on the screen, the object is also circling a location on the ground. As a result, we know that both the plane and object are circling the same location on the ground, approximately but the object's distance from the plane is unknown so its tangential velocity is not known exactly. From equation E6 by assuming perfect circular trajectories of average velocity it is possible to calculate the tangential velocity of the object as a ratio of the plane's radius about a center of rotation CR for a series of radii ranging from close to the CR to near the airplane's radius. This provides values of tangential velocities that can be compared to wind speed to see if the object is wind driven or must have some other means of propulsion. This is used as the basis for further calculations of objects tangential velocity as a function of distance from the plane's camera.

Since we don't have enough information to be able to calculate the instantaneous values of the tangential velocity, the average velocity serves as a bench mark that has the properties that although the tangential velocity may be lower at times than the average tangential velocity at other times it must be higher so that it can produce the measured average tangential velocity. This is shown in Figure A10 where the blue trajectories are the instantaneous velocity of the plane and the object but the red trajectories are the average velocity of the plane traveling in perfect circles about the center of rotation CR. Now we have to be able to take into account the error in the measured tangential velocity of the object due to the object being off of the co-radial trajectory shown in **Fig. A4** using equation E4. Further there is an unknown error in the instrument readings of the plane's ground speed *Vp* which can be difficult to estimate but from the author's research **[21]** this error is about 2.5% and is doubled to

5.0% as an extra conservative estimate. So, a ± 5% standard deviation is used for the instrument error. It is further assumed that the instrument error and the co-radial tangential velocity error are normally distributed and independent so that the mean errors can be added as well as the variances to produce a resultant normal distribution of both errors **[22].** The co-radial velocity error and the estimated instrument error will be used to produce a corrected co-radial tangential velocity to compare to wind speed at different altitudes to see if the wind could produce the trajectory observed in the RD2 video.

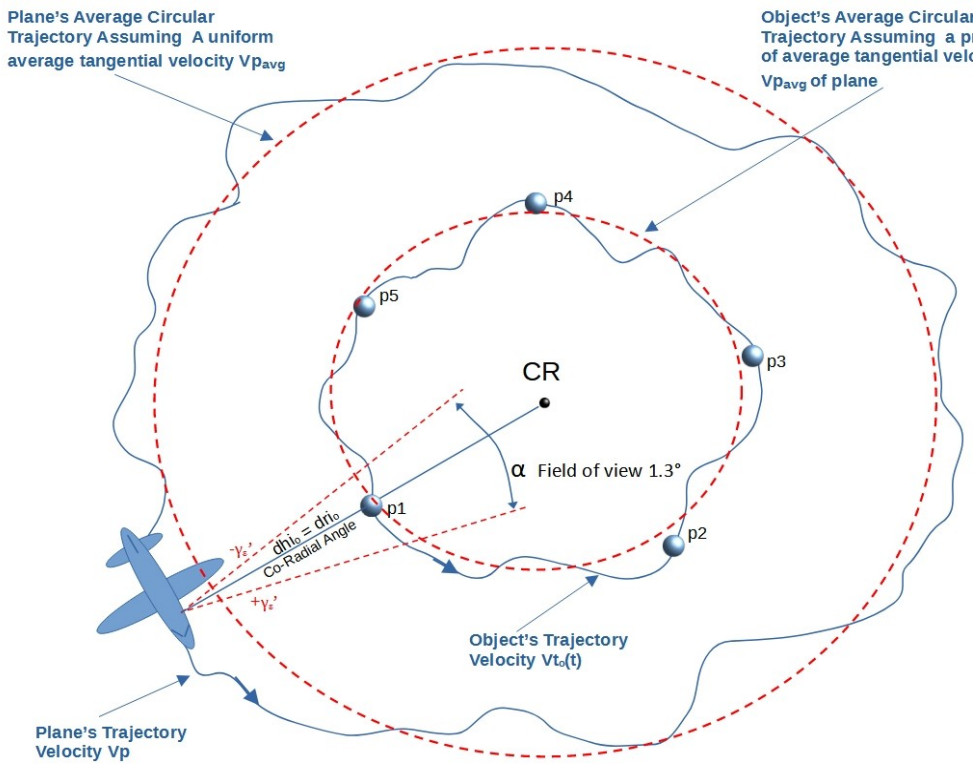

Figure A10: Shows the co-radial trajectory of the plane A - hi above the object and dhi$_o$ =dri$_o$ [See equation E2b] horizontally from the object, from a perspective looking down on the plane and the object, as it tracks the object circling some location on the ground both in red. In blue the average circular trajectory of the plane and object at a different altitude in blue, only one of many altitudes, hi, is shown for the object in blue, for simplicity.

	Plane Speed Vp Mph	Altitude ft	Object's co-radial Tangential Velocity	% Error from being non co-radial	Plane Speed Vp Mph	Altitude ft	Object's co-radial Tangential Velocity	% Error from being non co-radial	Plane Speed Vp Mph	Altitude ft	Object's co-radial Tangential Velocity	% Error from being non co-radial	Plane Speed Vp Mph	Altitude ft	Object's co-radial Tangential Velocity	% Error from being non co-radial
	197.80	14800.00	186.22	2.97	189.75	14798.00	171.63	4.89	217.35	14803.00	134.97	21.20	190.90	14801.00	189.97	0.24
	194.35	14791.00	187.27	1.84	213.90	14794.00	210.72	0.75	231.15	14803.00	111.54	30.53	190.90	14801.00	190.67	0.06
	213.90	14804.00	193.47	4.89	225.40	14803.00	210.30	3.41	244.95	14802.00	187.38	12.54	194.35	14800.00	188.49	1.52
	234.60	14805.00	232.04	0.55	241.50	14793.00	235.59	1.23	241.50	14803.00	241.21	0.06	204.70	14800.00	187.20	4.37
	247.25	14804.00	209.50	7.95	241.50	14800.00	234.22	1.52	221.95	14803.00	190.80	7.28	218.50	14801.00	195.34	5.45
	233.45	14803.00	228.93	0.97	234.60	14806.00	233.46	0.24	209.30	14805.00	160.11	12.54	232.30	14804.00	205.13	6.03
	203.55	14801.00	189.91	3.41	216.20	14795.00	213.84	0.55	209.30	14806.00	206.19	0.75	244.95	14804.00	232.55	2.56
	192.05	14804.00	186.26	1.52	192.05	14798.00	152.47	10.90	196.65	14796.00	186.70	2.56	248.40	14811.00	237.66	2.19
	190.90	14801.00	174.58	4.37	190.90	14799.00	190.38	0.14	189.75	14801.00	165.38	6.64	241.50	14814.00	237.91	0.75
	186.30	14782.00	186.30	0.00	188.60	14798.00	182.91	1.52	190.90	14803.00	172.67	4.89	226.55	14814.00	197.45	6.64
	201.25	14801.00	185.96	3.87	192.05	14789.00	189.95	0.55	192.05	14807.00	169.58	6.03	216.20	14817.00	190.91	6.03
	203.55	14804.00	177.41	6.64	215.05	14800.00	212.70	0.55	195.50	14800.00	137.51	16.13	216.20	14814.00	216.13	0.02
	228.85	14791.00	218.96	2.19	225.40	14806.00	210.30	3.41	207.00	14800.00	161.38	11.71	200.10	14804.00	192.81	1.84
	243.80	14804.00	243.13	0.14	244.95	14804.00	244.88	0.02	230.00	14800.00	227.49	0.55	192.05	14804.00	183.75	2.19
	242.65	14809.00	240.81	0.38	236.90	14811.00	226.66	2.19	246.10	14809.00	233.65	2.56	190.90	14798.00	185.14	1.52
	228.85	14802.00	227.74	0.24	215.05	14808.00	196.67	4.37	248.40	14809.00	243.59	0.97	193.20	14800.00	191.09	0.55
	200.10	14800.00	161.65	10.12	211.60	14806.00	199.22	2.97	242.65	14805.00	239.05	0.75	200.10	14801.00	199.86	0.06
	200.10	14802.00	199.86	0.06	190.90	14804.00	190.38	0.14	228.85	14804.00	223.25	1.23	209.30	14802.00	198.71	2.56
	187.45	14783.00	177.96	2.56	190.90	14801.00	159.32	8.65	210.45	14804.00	201.35	2.19	220.80	14801.00	187.09	7.95
	186.30	14804.00	180.68	1.52	204.70	14803.00	197.25	1.84	196.65	14802.00	189.49	1.84	233.45	14800.00	197.81	7.95
AVG:	210.85	14799.75	199.43	2.81	213.10	14800.80	203.14	2.49	217.52	14803.25	189.16	7.15	206.60	14804.55	200.28	3.02

	Object's co-radial Tangential Velocity	% Error from being non co-radial	Plane Speed Vp Mph	Object's Vt Velocity Mph	Object's co-radial Tangential Velocity	% Error from being non co-radial	Mean % error from being not co-radial	Standard Deviation σ % from being not co-radial	Assumed Standard Deviation σ % from Ground Speed Error	Combined Normal Distribution of % Errors Standard Deviation σ %
	199.43	2.81	210.85	204.98	199.43	2.81	3.87	5.03	5.00	7.09
	203.14	2.49	213.10	207.98	203.14	2.49				
	189.16	7.15	217.52	217.52	189.16	7.15				
	206.60	3.02	213.27	206.60	206.60	3.02				
AVG:	199.58	3.87	213.68	209.27	199.58	3.87				

*Figure A11: Calculation of % error in Vt_o of the object due to being off the co-radial angle γ' = 90° by $\pm$ γ'ε° with a standard deviation of 5.03% and an instrument ground speed error standard deviation of 5.00% which produces a final standard deviation of 7.09% for the combined sum of two normal distributed random variables due to independence. The mean is 3.87% co-radial error and 0% for the ground speed average error for a mean Vp of 213.68 Mph. Three Standard deviations about the mean will be used equal to 3*7.09 = 21.27% for a confidence level of 99.73% for a conservative estimate of the co-radial corrected Vt_o - this will be compared to the wind velocity to determine if the object could be propelled by the wind.*

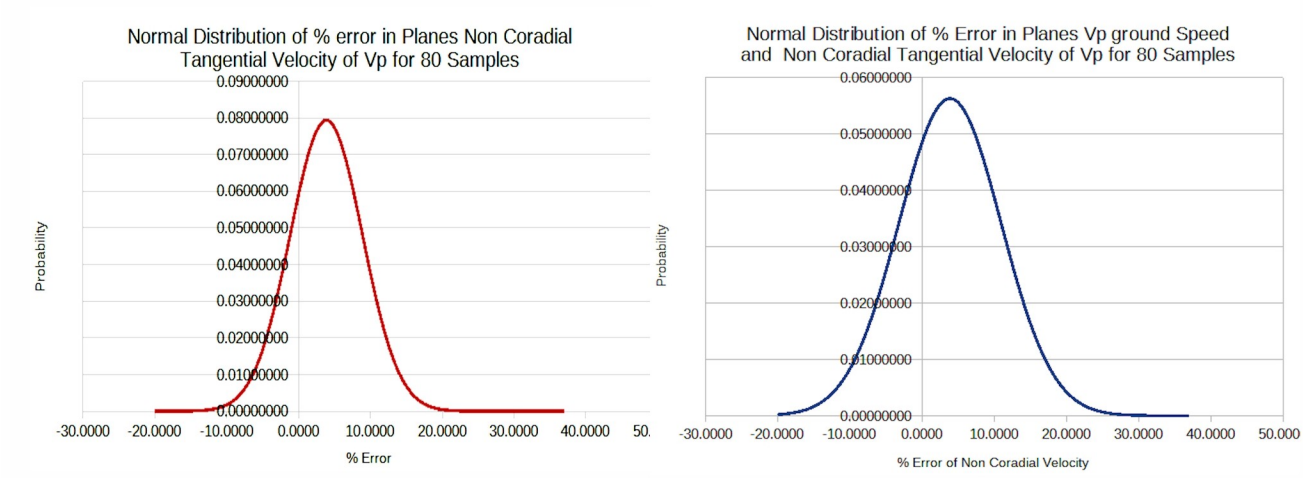

Figure A12: Comparison of the Normal distribution of the Co-radial error alone on the left in red and the Normal distribution of the Co-radial error and the estimated error of the ground speed on the right

5. Comparing the Tangential Velocity of the object to the local wind velocity at different altitudes: In our case the object is above ground and for the purpose of comparing the object's speed to the local wind velocity from atmospheric balloon sounding data as detailed in **Appendix B Sec. 4 (p. 28),** we use the lowest altitude of 750 ft as reported in the sounding data from Arizona State University as a starting point up to the altitude of the plane labeled A. We also know from the geographical terrain maps of the area that the object was flying above the San Louis Mountains that are 3750 ft in height. This is used to calculate the object's tangential velocity using equation E6 for various heights up to the plane's highest altitude as shown in figure A9. We then compare this to the atmospheric balloon sounding data for wind velocity on the date and time of the incident as shown in figure A13 to produce the graphs shown in Figure A15. It was further noted that the wind speed was compared to the previous day and following day and there was little variation compared to the day of the event. We can see in Figure A15 that the object's co-radial tangential velocity shown in yellow, taking into account angle pointing and instrument errors exceeds the wind velocity at all altitudes up to the plane. This means that a wind-blown object like a balloon or some other lighter than air object cannot be traveling at the velocity exhibited by the object in the RD2 video by wind forces alone.

Altitude Meters	Altitude Feet	Wind Velocity Knts	Wind Velocity Mph	Objects Uncorrected Co-radial Velocity Vt Mph	Objects Co-radial Corrected Velocity for 21.27% Errors Vto Mph	Wind Speed Mph Corrected for Possibl Instrument Errors of 30%
228.60	750.00	5.00	5.75	12.29	9.67	7.48
457.20	1500.00	5.00	5.75	24.58	19.35	7.48
685.80	2250.00	5.00	5.75	36.86	29.02	7.48
914.40	3000.00	8.00	9.20	49.15	38.70	11.96
1143.00	3750.00	7.00	8.05	61.44	48.37	10.47
1371.60	4500.00	6.00	6.90	73.73	58.04	8.97
1600.20	5250.00	6.00	6.90	86.01	67.72	8.97
1828.80	6000.00	4.00	4.60	98.30	77.39	5.98
2057.40	6750.00	7.00	8.05	110.59	87.07	10.47
2286.00	7500.00	8.00	9.20	122.88	96.74	11.96
2514.60	8250.00	6.00	6.90	135.16	106.41	8.97
2743.20	9000.00	8.00	9.20	147.45	116.09	11.96
2971.80	9750.00	12.00	13.80	159.74	125.76	17.94
3200.40	10500.00	18.00	20.70	172.03	135.44	26.91
3429.00	11250.00	25.00	28.75	184.31	145.11	37.38
3657.60	12000.00	26.00	29.90	196.60	154.78	38.87
3886.20	12750.00	27.00	31.05	208.89	164.46	40.37
4114.80	13500.00	28.00	32.20	221.18	174.13	41.86
4343.40	14250.00	29.00	33.35	233.46	183.81	43.36
4572.00	15000.00	29.29	33.68	245.75	193.48	43.79

Figure A13: Local wind velocity versus altitude in the area of the object and time of sighting compared to the average tangential velocity of the object calculated from equation E6 with error corrections for co-radial velocity of -21.27% and instrument wind speed errors of +30% assuming

Since the accuracy of the wind measuring instruments is unknown, we make the conservative assumption that it is normally distributed and could have a standard deviation of $\pm$10% and we take the most positive error case and for 3 standard deviations we use a +30% correction as shown in column 7 of figure A13 to make it as high as possible. This is shown as the upper wind speed in figure A15.

Altitude ft of Object hi	Vert Distance From Camera to Object ft vdi	Horiz Distance From Camera to Object ft vdi = dh $\beta = -17_{deg}$	Slant Diagonal Distance Sdd ft With α deg angle down	Field of View at Object ft or Span = Si	RTF Reticle Field of View ft	Object Size Ft	Approx Object Tangential Velocity mph Vt using Vert Dist	Approx Object Tangential Velocity mph Vt Horiz Dist	Maximum Horizontal Distance at 15000 ft from Camera
750.00	14,250.00	40,406.73	48,739.33	1,105.91	184.32	11.52	12.29	12.29	51,304.55
1,500.00	13,500.00	38,280.06	46,174.10	1,047.70	174.62	10.91	24.58	24.58	51,304.55
2,250.00	12,750.00	36,153.39	43,608.87	989.50	164.92	10.31	36.86	36.86	51,304.55
3,000.00	12,000.00	34,026.72	41,043.64	931.29	155.22	9.70	49.15	49.15	51,304.55
3,750.00	11,250.00	31,900.05	38,478.42	873.09	145.51	9.09	61.44	61.44	51,304.55
4,500.00	10,500.00	29,773.38	35,913.19	814.88	135.81	8.49	73.73	73.73	51,304.55
5,250.00	9,750.00	27,646.71	33,347.96	756.67	126.11	7.88	86.01	86.01	51,304.55
6,000.00	9,000.00	25,520.04	30,782.73	698.47	116.41	7.28	98.30	98.30	51,304.55
6,750.00	8,250.00	23,393.37	28,217.50	640.26	106.71	6.67	110.59	110.59	51,304.55
7,500.00	7,500.00	21,266.70	25,652.28	582.06	97.01	6.06	122.88	122.88	51,304.55
8,250.00	6,750.00	19,140.03	23,087.05	523.85	87.31	5.46	135.16	135.16	51,304.55
9,000.00	6,000.00	17,013.36	20,521.82	465.65	77.61	4.85	147.45	147.45	51,304.55
9,750.00	5,250.00	14,886.69	17,956.59	407.44	67.91	4.24	159.74	159.74	51,304.55
10,500.00	4,500.00	12,760.02	15,391.37	349.23	58.21	3.64	172.03	172.03	51,304.55
11,250.00	3,750.00	10,633.35	12,826.14	291.03	48.50	3.03	184.31	184.31	51,304.55
12,000.00	3,000.00	8,506.68	10,260.91	232.82	38.80	2.43	196.60	196.60	51,304.55
12,750.00	2,250.00	6,380.01	7,695.68	174.62	29.10	1.82	208.89	208.89	51,304.55
13,500.00	1,500.00	4,253.34	5,130.46	116.41	19.40	1.21	221.18	221.18	51,304.55
14,250.00	750.00	2,126.67	2,565.23	58.21	9.70	0.61	233.46	233.46	51,304.55
15,000.00	0.00	82.90	100.00	2.27	0.38	0.02	245.75	245.27	51,304.55

Figure A14 Preliminary calculations of Size and Tangential Velocity of Object for β angle of -17°

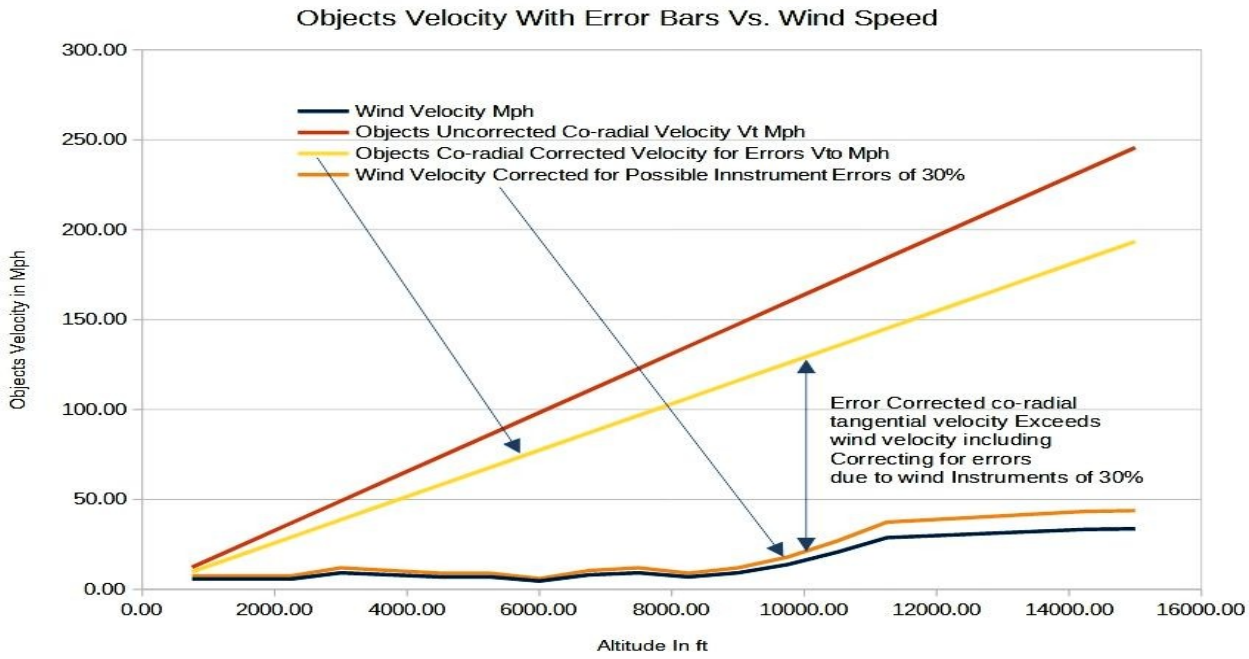

Figure A15: Tangential velocity Vt of object compared to local wind velocity at different altitudes with 3 standard deviations of error with 21.27% co-radial velocity and 30% wind speed instrument

6. Size of the object:
Shown in Figure A16, the size of the object vs the height above ground level. The object's size depends on the vertical distance from the plane and the β angle, it can be as large as 38 ft near the ground or as small as 1 ft or less if very near the plane. It appears that the object is above the local San Louis Mountains which range up to 3750 ft **[8]** and using an average β angle of -17°, it is estimated to between 1 to 9 ft in length. See **Appendix D Sec. 3 (p. 37) for a deeper analysis based on pixel size.** The distance from the plane is unknown but an object smaller than 1 ft is probably unlikely to not be seen in detail by the telescopic capability of the FLIR camera **[Appendix A Sec. 1 (p. 10)].**
The size of the object in Figure A14 column 7 is calculated from the RFV "reticle field of view" in feet in column 6 from the derivations shown above for Spn, the RFV is 1/6th of the total field of view. Taking the proportion P of the object occupying the RFV proportion of the screen. This was found to be 1/16 of the screen width. So, the size of the object, Os is calculated as

Os = Sp*RFV*P $=\frac{Sp}{(6*16)}=\frac{Sp}{96}$ in ft and this was used to make Column 7 in figure A14. Figure A16 lets the size be a function of the diagonal distance Sddn and β angle and gives a wide range of possible sizes. The screen's full horizontal dimension in pixels should be a proportional representation of the span distance Sp_n shown in Figure A3. We can write: $Os = Spn * RFV * P$

and solving for Spn $$Spn=\frac{Os}{(RFV*P)}$$ E7

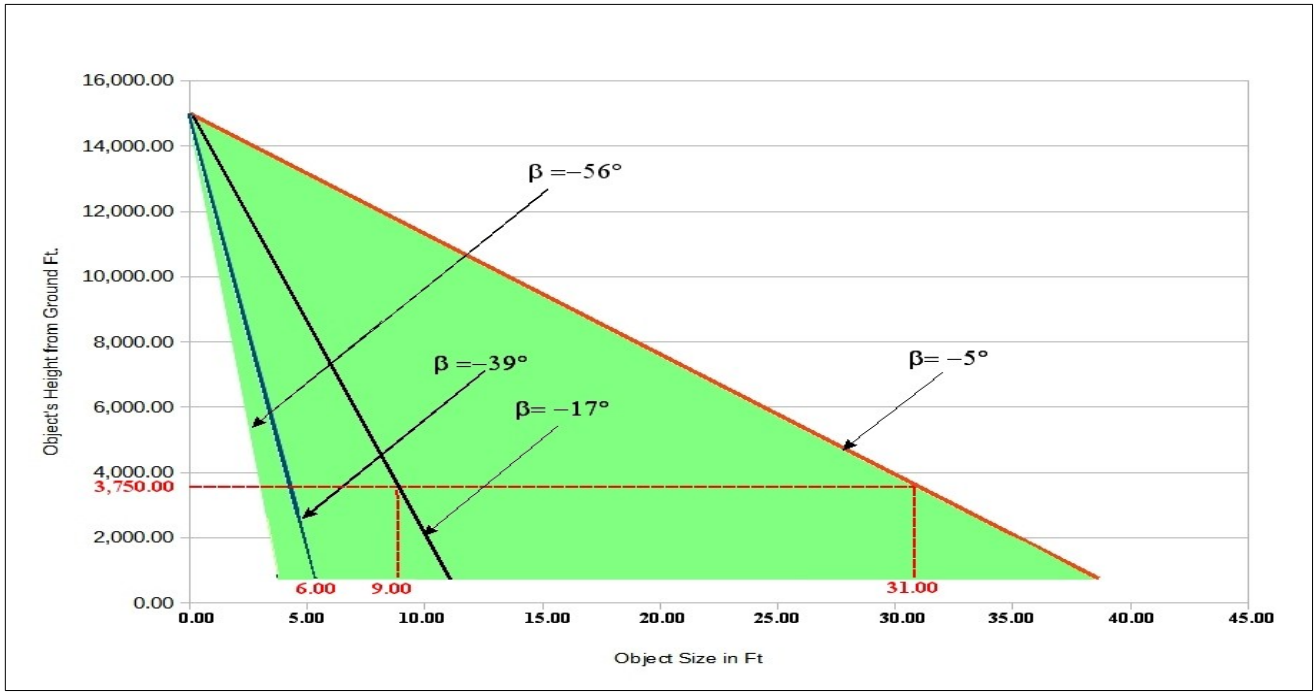

Figure A16 Size of Object vs Object's height above ground and β angle of camera

Figure A5 shows 3 positive β angles of (+3, +2 and +2)° and Fig A6 shows one β angle that is +5° but Figure A16 has all negative β angles. Figure A17 shows that as the plane banks left to turn, a positive angle can be recorded because the camera records β angles relative to the plane's horizontal axis and

not the geographical horizon **[Appendix C #11. (14), (p. 32)]** resulting in a positive angle. In the actual video the object is

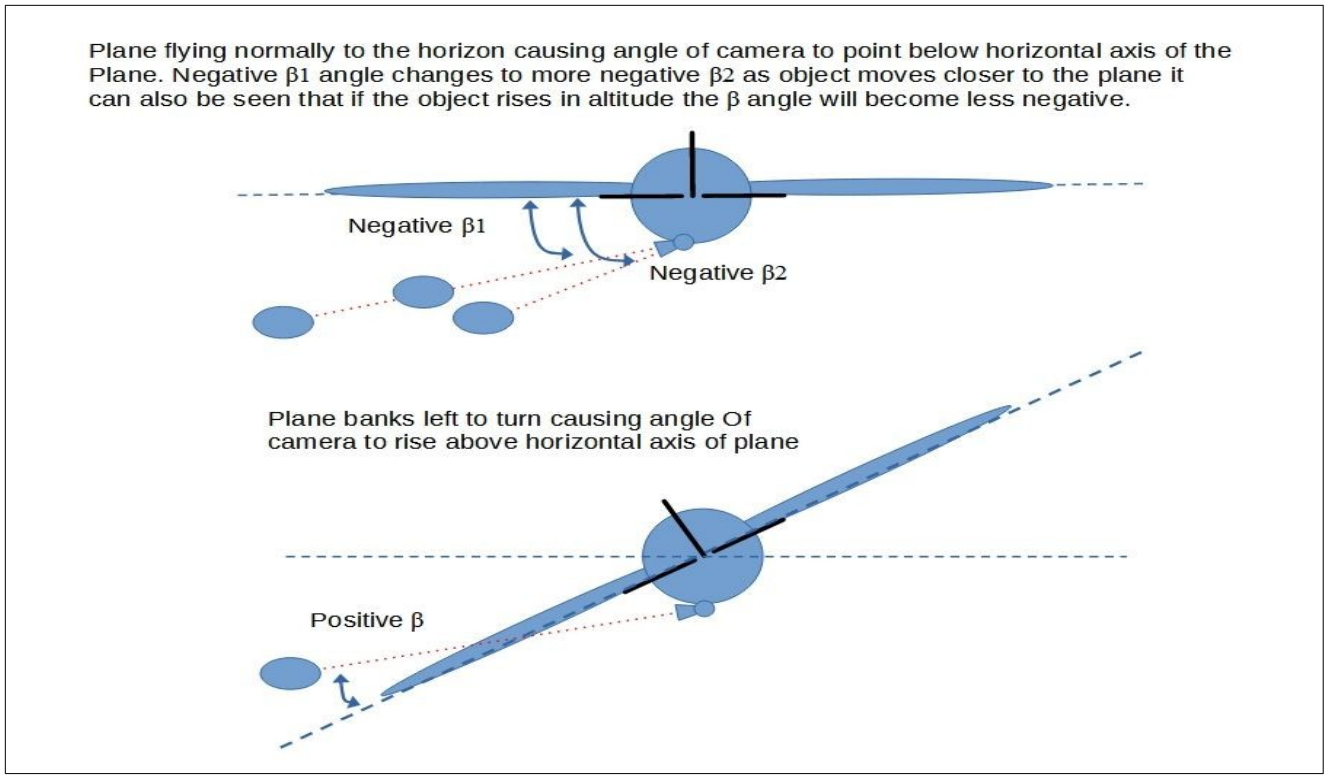

Figure A17 β angles can change due to changes in horizontal and vertical distances from the plane's axis and Positive β angles occur when plane banks to turn

clearly below the plane and the horizon is never visible indicating that the camera never points above the actual horizon. To compensate for this in the calculations a -7.5° offset is used to keep all the angles negative and well below the horizon, as the average β angle is -17.82°. This is necessary as there is no actual knowledge of the plane banking angle with respect to the horizon and this seems like a reasonable assumption for the calculations resulting in Figure A16. The altitude of the object in the RD2 video is seen to be well above the western edge San Louis Mountain ranges in the Buenos Aires National Wild Life Refuge **[Appendix E Sec. 2, Fig E3 (p. 43),]** which can rise to 3,750 ft **[8]** so the most likely altitudes are between 3,750 to 14,000 ft. This is indicated by the dashed red line intersecting the -17° β angle locus in Figure A16.

Appendix B: Analysis of the cause of anomalous temperature indications in the RD2 video.

1. The objects anomalous characteristics with regard to temperature:
The object was recorded using an infrared camera of the Star SAFIRE-380 camera family made by Teledyne Systems and is sensitive to the Medium Infrared (MIR) spectrum with
Camera Specifications **[6]:**

Thermal Imager:

Sensor type	1280 x 720 InSb MWIR FPA (standard) 640 x 512 InSb MWIR FPA (optional)
Resolution	720p/1080p HD and NTSC/PAL
Wavelength	3-5 µm response
FOVs	40° to 0.35° (with standard FPA)
Zoom ratio	120x

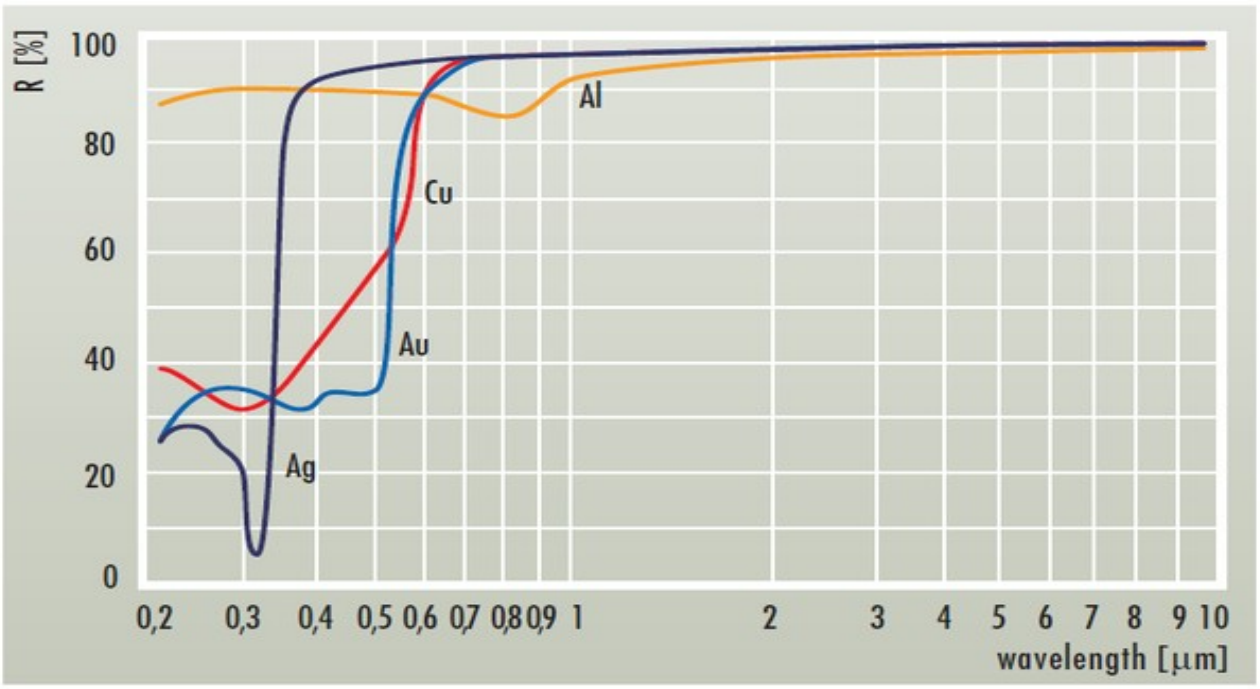

Figure B1: Infrared reflection characteristics for different metals

2. Observed characteristics of the object with respect to temperature:
The object remains cold compared to the surrounding environment which would be the atmospheric gasses of Oxygen and Nitrogen and the exposure to the clear night sky. The fact that an object appears cold is not anomalous in itself as most metallic objects could appear this way as a result of their reflective nature at mid-infrared wavelengths. The SCU has done experiments to demonstrate this in a reference video. **[7]** Exceptions to this occur with images of fast-moving metallic objects like airplanes which get heated by air friction causing them to radiate infrared radiation that overcomes the reflected radiation that would normally be detected. A slow-moving object like a metallic coated balloon could appear colder than the surroundings from above as it would reflect the night sky's temperature.

We start with the three possible types of misidentified objects that the camera could be recording:

1. The object could be a lighter than air object like a weather balloon, Mylar party balloon or parachute or some fabric being blown in the wind. Further Mylar nylon balloons are not used for weather balloons as they will break from the pressure differential when rising to an altitude of between 3,000 to 8,000 ft **[13].** Latex is used for weather balloons which can rise to 100,000 ft before exploding. Latex is transparent to infrared and would transmit the ground temperature as the camera is looking down from the aircraft **[7]**. The object cannot be a weather balloon. Further any other object being blown by the wind is slower than the calculated tangential velocity of the object showing it cannot be driven by the wind as shown in **Appendix A Sec. 5, Figs. A14, A15 (p.23)** derived above. **Figs. B3, B4 (p. 29, 30)** below show the raw data for wind velocity. Further, if it were a balloon, it should present a varied shape as it is blown by the wind and rotates, as will be discussed in **Appendix D Sec. 1 (p. 34).**

2. The object could be a small unmanned object like a drone. Drones come in two types of configurations: A small airplane like aerodynamic structure with wings and a motor or vertical lift type configurations with quad or even more motors that can be either electric or gas powered. Not having wings means all the energy of the engines are used just to give it lift and a modest amount of forward thrust. The battery powered ones have very limited flight times of about 30 minutes but the

Figure B2: Infrared signature of a plane showing the heat of the exhaust from the engine and the airframe being heated by friction.

gas-powered industrial drones can go much longer like helicopters **[17].** The shape of the object rules out the aerodynamic type of drone as is explained in more detail in **Appendix D Sec. 1 (p. 34)** and **Appendix F Sec. 6 (p. 46)**. Battery powered devices don't have the endurance that the object displays in the video, where between the two videos it is airborne for at least 45 minutes and in their executive summary. **Appendix F Sec. 7 (p. 46)** the pilots describe first seeing the object as it came

in from flying over the Mexican border into Arizona. Gas powered quad, hex or octo-copters would show prominent heat signatures for the engines that don't appear in the videos. Further even battery powered drones can show the battery as being warmer than the environment. None of these possibilities are consistent with the cold temperature depicted in the infrared video recording.

3. The object could be a conventional powered plane or unpowered sail plane. Similar to the drones a plane would have aerodynamic structures that are not displayed in the video. A conventional airplane's engines would appear hotter than the surroundings and the body would also be hotter due to air friction. A sail plane would appear as the same temperature as its surroundings and not be colder. Figure B2 shows and example of this.

3. SCU experimental tests of conventional Latex and Mylar balloons with infrared cameras:
The SCU has conducted tests using metallic coated balloons and mirrors that show these characteristics that can be seen in the videos **[7].** For an object to be colder than its surrounding environment it must be totally reflective at the 3-5um infrared wavelengths recorded by the camera. Figure B1 **[9]** shows the infrared reflection characteristics of different metals and all of them are very good reflectors of Infrared radiation at the 3-5um response of the FLIR camera. In the cited video you can see that a conventional balloon is nearly transparent to infrared radiation and objects can be seen behind the balloon. This rules out balloons as an explanation for the observed characteristics displayed in the video.

4. Weather Data:
Figure B3 **[11]** shows at the time of the incident the weather was clear and winds were mild at less than 10 mph at ground level. Winds could be higher at higher altitudes but not enough to account for the tangential velocities as derived in **Appendix A Sec. 5 (p. 22) Figs. A13 and A15** previously. Figure B4 shows that wind velocity on the night of the incident at higher altitudes was a maximum of 33 mph near the plane and much less below it, confirming this conclusion. Weather in the RD2 video appears clear and no mention of adverse weather was reported by the airplane crew in **Appendix F (p. 44).**

U.S. Department of Commerce
National Oceanic & Atmospheric Administration
National Environmental Satellite, Data, and Information Service

Local Climatological Data
Hourly Observations
November 2019
Generated on 06/21/2021

National

Current Location: Elev: 2549 ft. Lat: 32.1313° N Lon: -110.9552° W
Station: **TUCSON INTERNATIONAL AIRPORT, AZ US WBAN: 72274023160 (KTUS)**

Date	Time (LST)	Station Type	Sky Conditions	Visibility	Weather Type (see documentation)	Dry Bulb Temp		Wet Bulb Temp		Dew Point Temp		Rel Hum %	Wind Speed (MPH)	Wind Dir (Deg)	Wind Gusts (MPH)	Station Press (inHg)	Press. Tend	Net 3-Hr Chang (inHg
					AU I AW I MW	(F)	(C)	(F)	(C)	(F)	(C)							
1	2	3	4	5	6	7	8	9	10	11	12	13	14	15	16	17	18	19
23	0053	7	CLR:00	10.00		49	9.4	46	7.8	43	6.1	80	0	000		27.48		
23	0153	7	CLR:00	10.00		46	7.8	44	6.7	41	5.0	83	3	150		27.48	8	+0.01
23	0253	7	CLR:00	10.00		45	7.2	43	6.1	41	5.0	86	3	120		27.47		
23	0353	7	CLR:00	10.00		45	7.2	43	6.1	40	4.4	83	3	210		27.47		
23	0453	7	CLR:00	10.00		43	6.1	41	5.0	39	3.9	86	0	000		27.45	6	+0.02
23	0500	4		9.94		43	6.1	41	5.0	39	3.9	86	0	000		27.43	6	+0.02
23	0553	7	CLR:00	10.00		44	6.7	42	5.6	39	3.9	83	3	140		27.47		
23	0653	7	CLR:00	10.00		46	7.8	44	6.7	41	5.0	83	0	000		27.47		
23	0753	7	CLR:00	10.00		47	8.3	45	7.2	42	5.6	83	0	000		27.49	1	-0.03
23	0853	7	CLR:00	10.00		55	12.8	47	8.3	39	3.9	55	8	090		27.49		
23	0953	7	CLR:00	10.00		60	15.6	49	9.4	37	2.8	42	16	130		27.50		
23	1053	7	CLR:00	10.00		64	17.8	50	10.0	37	2.8	37	17	130		27.48	8	+0.01
23	1100	4		9.94		64	17.8	50	10.0	37	2.8	37	17	130		27.46	8	+0.01
23	1153	7	CLR:00	10.00		65	18.3	51	10.6	38	3.3	37	10	140		27.46		
23	1253	7	CLR:00	10.00		67	19.4	52	11.1	37	2.8	33	9	140		27.44		
23	1353	7	CLR:00	10.00		69	20.6	52	11.1	36	2.2	30	8	090		27.41	8	+0.07
23	1453	7	CLR:00	10.00		71	21.7	52	11.1	34	1.1	26	5	VRB		27.39		
23	1553	7	CLR:00	10.00		70	21.1	51	10.6	33	0.6	26	5	030		27.39		
23	1653	7	CLR:00	10.00		66	18.9	52	11.1	39	3.9	37	6	350		27.39	5	+0.02
23	1700	4		9.94		66	18.9	52	11.1	39	3.9	37	6	350		27.37	5	+0.02
23	1753	7	CLR:00	10.00		61	16.1	51	10.6	42	5.6	50	6	270		27.41		
23	1853	7	CLR:00	10.00		58	14.4	51	10.6	44	6.7	60	3	260		27.41		
23	1953	7	CLR:00	10.00		57	13.9	50	10.0	44	6.7	62	0	000		27.42	1	-0.03

Figure B3: Weather data from the time of the incident showing very low wind speeds and clear weather near ground level. The instruments used by the Balloon sounding data instruments are conservatively estimated as ± 10% standard deviation of error.

5. Conclusions regarding temperature:

It would appear the object reflects as if it were made of metal or has a characteristic surface that acts in a similar fashion as if it were constructed of metal. The low velocity of the metal object might account for a colder infrared signature. The rigidity of the object would be consistent with a metallic structure but the shape and lack of any visible propulsion system makes it truly anomalous when considering that all know propulsion systems would appear hotter than the surrounding environment.

72274 TUS Tucson Observations at 12Z 23 Nov 2019

Dashed Red Line represents highest altitude of the plane at about 15,000 ft or 4,572 m

PRES hPa	HGHT m	TEMP C	DWPT C	RELH %	MIXR g/kg	DRCT deg	SKNT knot	THTA K	THTE K	THTV K
1000.0	166									
933.0	751	7.6	5.7	88	6.19	200	2	286.4	303.9	287.4
925.0	824	8.4	6.4	87	6.56	165	2	287.9	306.6	289.0
919.0	878	8.8	6.3	84	6.55	144	3	288.8	307.6	290.0
915.0	914	9.3	5.7	78	6.32	130	4	289.7	307.9	290.8
906.0	996	10.4	4.4	66	5.82	115	7	291.7	308.6	292.7
892.0	1126	10.0	3.0	62	5.35	92	11	292.6	308.3	293.5
884.0	1201	10.8	0.8	50	4.61	78	13	294.1	307.9	294.9
882.1	1219	10.8	0.6	49	4.55	75	14	294.3	307.9	295.1
862.0	1411	10.4	-1.6	43	3.96	84	10	295.8	307.8	296.6
850.0	1527	9.6	-0.4	50	4.39	90	7	296.2	309.4	297.0
833.0	1694	8.2	0.2	57	4.68	107	5	296.4	310.5	297.3
819.5	1829	7.5	-0.5	57	4.53	120	3	297.1	310.8	297.9
802.0	2007	6.6	-1.4	57	4.33	143	5	297.9	311.1	298.7
789.7	2134	6.7	-8.5	33	2.56	160	7	299.4	307.5	299.9
785.0	2183	6.8	-11.2	26	2.08	156	7	300.0	306.6	300.4
764.0	2405	5.6	-18.4	16	1.18	138	10	301.0	304.9	301.2
760.9	2438	5.4	-18.5	16	1.18	135	10	301.2	305.1	301.4
732.8	2743	4.0	-19.1	17	1.16	345	1	302.9	306.8	303.1
700.0	3115	2.2	-19.8	18	1.14	255	2	304.9	308.7	305.1
684.0	3301	1.0	-22.0	16	0.97	251	2	305.6	308.9	305.8
679.6	3353	1.0	-23.8	14	0.83	250	2	306.1	308.9	306.2
664.0	3539	0.8	-30.2	8	0.47	259	5	307.9	309.6	308.0
654.2	3658	-0.1	-32.2	7	0.39	265	7	308.2	309.7	308.3
646.0	3758	-0.9	-33.9	6	0.34	269	10	308.4	309.7	308.5
626.0	4009	-1.3	-32.3	7	0.41	279	18	310.8	312.3	310.9
615.0	4149	-2.3	-14.3	39	2.07	285	22	311.2	318.1	311.6
605.9	4267	-3.0	-13.8	43	2.18	290	26	311.7	318.9	312.1
593.0	4437	-4.1	-13.1	50	2.36	289	29	312.4	320.2	312.8
572.0	4721	-5.3	-22.3	25	1.12	286	34	314.2	318.1	314.4
566.0	4803	-6.1	-19.1	35	1.50	286	36	314.2	319.4	314.5
562.0	4859	-6.7	-15.7	49	2.01	285	37	314.1	320.9	314.5
560.7	4877	-6.8	-15.7	49	2.02	285	37	314.2	321.0	314.6
553.0	4984	-7.7	-15.7	53	2.05	283	38	314.4	321.3	314.8
549.0	5041	-8.1	-16.1	53	1.99	282	39	314.6	321.3	315.0
546.0	5083	-8.1	-21.1	34	1.31	282	39	315.1	319.6	315.3
543.0	5126	-8.5	-20.5	37	1.39	281	39	315.1	319.9	315.4
539.1	5182	-8.8	-24.2	28	1.01	280	40	315.4	319.0	315.6
535.0	5241	-9.1	-28.1	20	0.71	279	40	315.7	318.3	315.9
524.0	5401	-10.1	-23.1	34	1.14	278	39	316.4	320.4	316.6
517.0	5504	-10.9	-31.9	16	0.51	277	38	316.6	318.5	316.8
507.0	5654	-12.1	-27.1	28	0.82	276	38	317.0	319.9	317.1
500.0	5760	-13.1	-29.1	25	0.69	275	37	317.0	319.5	317.1
495.0	5836	-13.7	-21.7	51	1.37	275	37	317.2	322.0	317.4
478.3	6096	-16.1	-23.4	53	1.22	275	39	317.4	321.7	317.6
471.0	6212	-17.1	-24.1	55	1.16	275	40	317.5	321.6	317.7
463.0	6340	-17.7	-26.7	45	0.94	274	42	318.3	321.7	318.5
457.0	6438	-18.3	-27.3	45	0.90	274	43	318.8	322.0	318.9
448.0	6586	-18.7	-33.7	25	0.50	273	45	320.1	321.9	320.2
446.0	6619	-18.9	-30.9	34	0.66	273	45	320.2	322.6	320.4
428.0	6925	-21.5	-28.5	53	0.86	272	49	320.7	323.8	320.9
424.0	6994	-21.9	-30.9	44	0.69	272	50	321.1	323.6	321.2

Figure B4: Weather balloon sounding data showing wind speed and temperature at different altitudes. The red dotted line shows the maximum altitude of the plane. The right green dotted area shows the maximum wind velocity as 29 kts or 33 mph. These figures were used to construct Figure A14. Balloon Sounding data for the previous and subsequent days were similar in velocity for the wind. The instruments used by the Balloon sounding data instruments are estimated as having a ± 10% standard deviation of error.

Appendix C: Definitions of the metadata on the video screen of the Star SAFIRE 380 HD FLIR camera from research conducted by the SCU, is incomplete and some meta data remains undefined due to the fact that it is often proprietary and difficult to obtain. Essential metadata is correct.

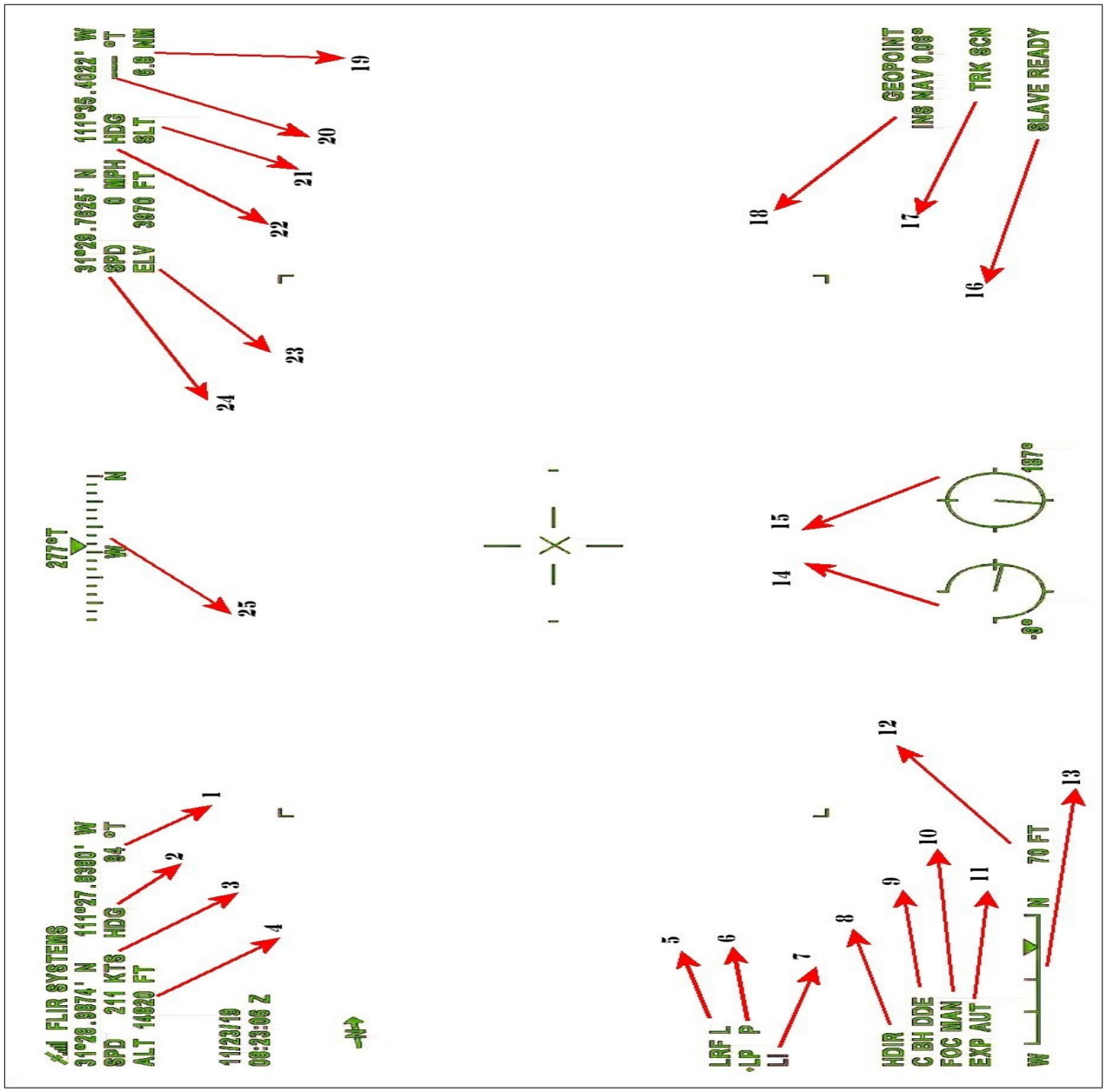

Figure C1: Star SAFIRE-380 HD FLIR Camera Meta Data Index

Understanding the definitions of the metadata presented by the FLIR camera is critical to understanding how to analyze the kinematics displayed by the object in the video. Numbers shown in square brackets (**N)** refer to the metadata pointed to by red arrows in Figure C1.

1. **(1)**. The true heading (not magnetic) of the airplane direction of travel called **"Platform Data" (20)**. The true direction of the camera angle. Called **"Target Data"**

2. **(2)** and **(22)** are labeled **HDG** for "heading metadata" at **(1)** and **(20). shown above HDG as 31°.0074'N and 111°.0900' W**

3. **(3)** and (**24)** 3 is speed in knots of the airplane with respect to ground and **24** is the speed of the target acquired by means of the **LRF** (laser Range Finder) and triangulation.

4. **(4)** and (**23)**, **4** is the altitude of the plane with respect to ground in ft and **23** is the elevation of target with respect to the ground once it is acquired by **LRF** and triangulation.

5. **(5) LRF L** is the Laser Range Finder in longest pulse mode.

6. **(6) LP P** indicates the Laser Pointer Pulse Mode.

7. **(7)**. **LI** indicates Laser Illuminator function.

8. **(8, 9, 10, 11) (HDIR** is high-definition illuminator**), (C** is cold scene temperature setting**),**

(BH Black Hot Mode**)** objects shown in black are colder than white objects**,** (**DDE** digital detail enhancement**)**

9. **(12)** shows **70 FT** Distance between Reticle Marks if **LRF** is active. If active a red indicator should be showing.

10.**(13)** is one of the 5 field of view modes of the camera pointed by a downward triangle with 5 divisons between **W----|----\|/----|----N** the center division is **narrow** as defined below:

Sensor 640x512	Field of View α FOV deg	Focal Length mm	Sensor 1280x720	Field of View α FOV deg	Focal Length mm
Wide	**30**	**24**	**Wide**	**40**	**24**
Medium	**4.9**	**150**	**Medium**	**6.9**	**150**
Narrow	**0.9**	**800**	**Narrow**	**1.3**	**800**
Super Narrow	**0.5**	**1464**	**Super Narrow**	**0.7**	**1464**
Ultra Narrow	**0.25**	**2928**	**Ultra Narrow**	**0.35**	**2928**

and **(25)** shows compass true North heading direction of the Airplane called the **"The Heading Tape"**

11. **(14)** and **(15) 14** is the vertical angle **β** below the nose of the aircraft **and not the geographic horizon parallel to the ground plane** that the camera is pointing to, **15** is the horizontal angle **γ** the camera is pointing to from the aircraft nose or ***azimuth*** **with respect to the plane and not the geographic horizon parallel to the ground plane**.

12. **(16)** is **SLAVE READY,** the camera is ready to slave to an external device, **(17) TRK SCN** there are a variety of tracking options, **(18) GEOPOINT INS NAV 0.06°** indicates the accuracy of the heading and triangulation indications.

13. **(19) and (21)** 6.0 NM reading: Slant range to target when locked with laser or by triangulation using mapping information and lens field of view.

14. Calculation of the magnification factor of narrow in item 10 above:
The telescopic capability of the camera is not covered in the paper but for the narrow setting of the camera as mentioned previously we can estimate the telescopic capability of the setting as the ratio of the narrow field of view of 1.3° to the wide field of view of 40° **[Appendix C, #10, column 5 (p. 32)]**

$\frac{40}{1.3} = 32\,X$ magnification which would make a close-up object have observable detail.

Appendix D: Examination of the possible origins of the object shape and the effect of pixel resolution in the RD2 video assuming the object has definite structure and is not some type of luminous plasma phenomenon.

1. Possible shape conjectures based on image resolution and the airplane's camera perspective: A possible explanation of the object based solely on shape is shown in figure D1. This assumes that the large object is on top of the small object. On the left we see a typical latex weather balloon and on the right a hypothetical view of the balloon looking up from below contrasted with looking at the balloon from above which occurs in RD2, the plane's video. The right view shows at the top a rather deflated balloon and at the bottom a less deflated balloon at low pixel resolutions. It does bear some striking similarities to the object in the video.

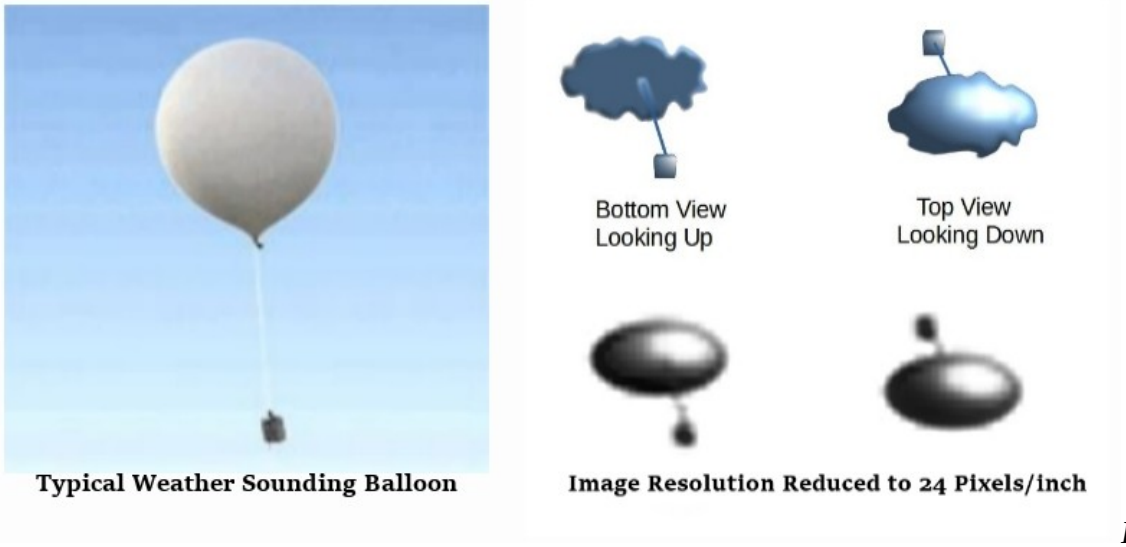

Figure D1: Left Image is a typical weather balloon and right images show a deflated balloon as it might appear from the ground or looking down from the plane and the bottom right images show a low-resolution image of a deflated balloon from ground level and looking down from the plane.

While there is some resemblance to a deflated balloon, as the image is viewed in the RD2 video, it can be seen that the object appears to be rather rigid in shape and does not ripple or flutter as one would expect when blown by the wind, see **[7].** Further as the object moves over the landscape, the bottom portion of the object swings in a pendulum type of motion at an extremely slow rate as it moves out of sight below the object and then eventually returns to its original position. This would indicate a very low and steady wind velocity if it were a weather balloon. Some of this motion may be due to changes in the planes viewing angle due to the object changing altitude or the plane moving closer or farther from the object in the horizontal plane as it follows the object with its camera as demonstrated in **Fig. A17**. This would imply that the object is even more rigid. It is also significant that the bottom object is quite large compared to the top of the object which is uncommon in weather balloons as shown in

figure D1 on the left. One cannot rule out that it is not some type of specialized balloon experiment based on the shape alone. **[Appendix F Sec. 6 (p. 46)]** gives the pilots account that the object traveled against the wind with no effort and that it appeared in infrared sensors as colder than the surrounding environment and gave off no heat signature from any power source as a means of propulsion; further, its shape from the video is completely non-aerodynamic. The pilot believed the object to be a balloon with the larger object on top but it was never seen optically only on the infrared camera's screen.
It can't be ruled out that the large object is not below the small object as it is difficult to tell from the video resolution which case is true. If the large object is below the small object, then we have a truly anomalous shape that is not compatible with any known aerodynamic shapes. A possibility is a deflated balloon is being suspended by a more buoyant smaller balloon but this seems difficult to classify.

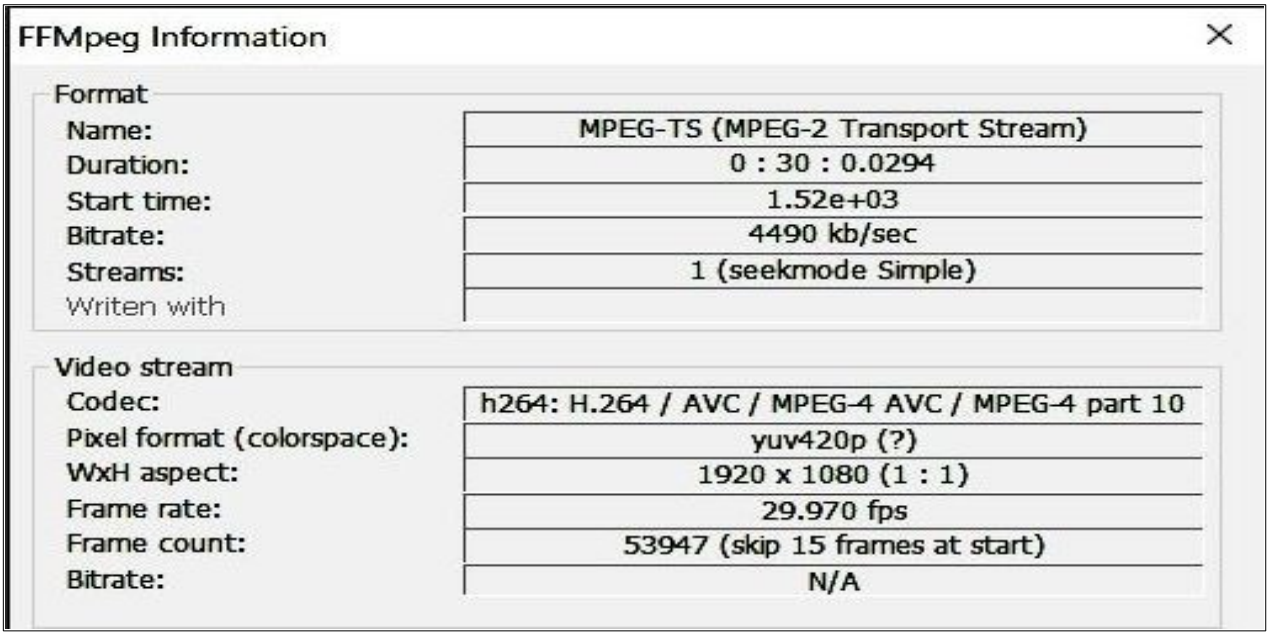

Figure D2: RD2 video format information is shown as a resolution of 1920 x 1080 which must be upscaled from the sensor resolution of 1280 x 720 as shown in ***Appendix C 10 column 4 (p. 32).***

2. Examination of the Pixel resolution of the RD2 video

Figure D2 shows the RD2 video sensor resolution from the metadata as being HD video with an up scaled horizontal resolution of 1920 pixels and a vertical resolution of 1080 pixels. This is a rather small sensor and makes distant objects very small in pixel resolution.

We perform an analysis of the pixel resolution of the object images from the RD2 video to estimate the capability of determining the shape of the object.

The image shown in Figure D3 is a screen capture of the object zoomed up by 2000% showing the approximate horizontal dimension of the object as 23 pixels. The object appears to have no known aerodynamic shape but could this be due to the low resolution of the image?

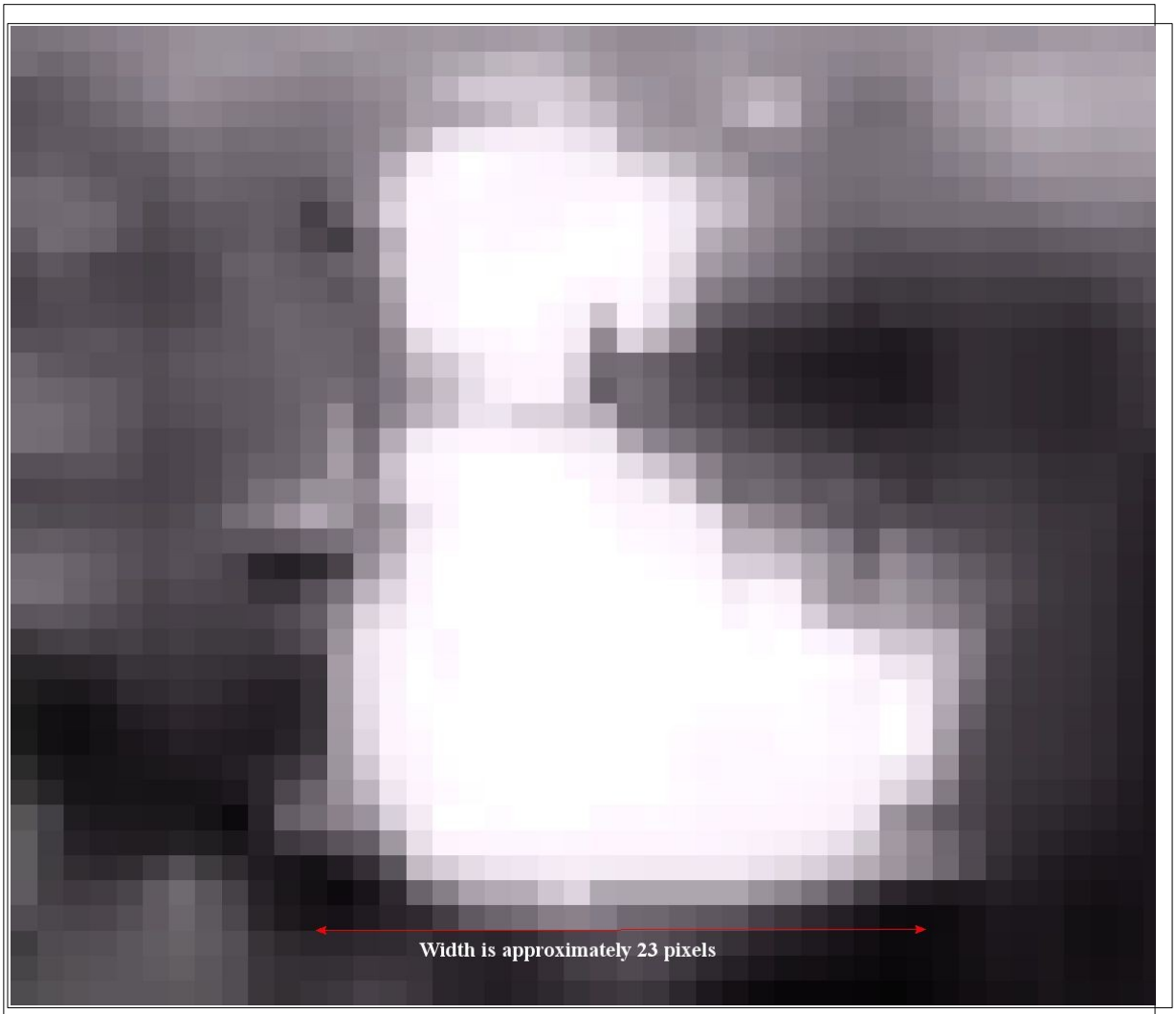

Figure D3: Zooming image by 2000% to show the horizontal dimension of the object in

The small number of pixels and the limited bandwidth of the sensor does not allow for much more information about the object from its image. If the camera had been zoomed into a higher telescopic range it might have shown more details about the object but this may have made it much harder to manually track the object. It was reported that the object was not visible to the pilot's eyes but this may be due to the distance to the object and the fact it was two hours after midnight at the time of the observation. If the plane could have flown closer to the object this would have provided a much better image but this may have been prevented by the restricted procedures that the pilots and crew must adhere to on a mission.

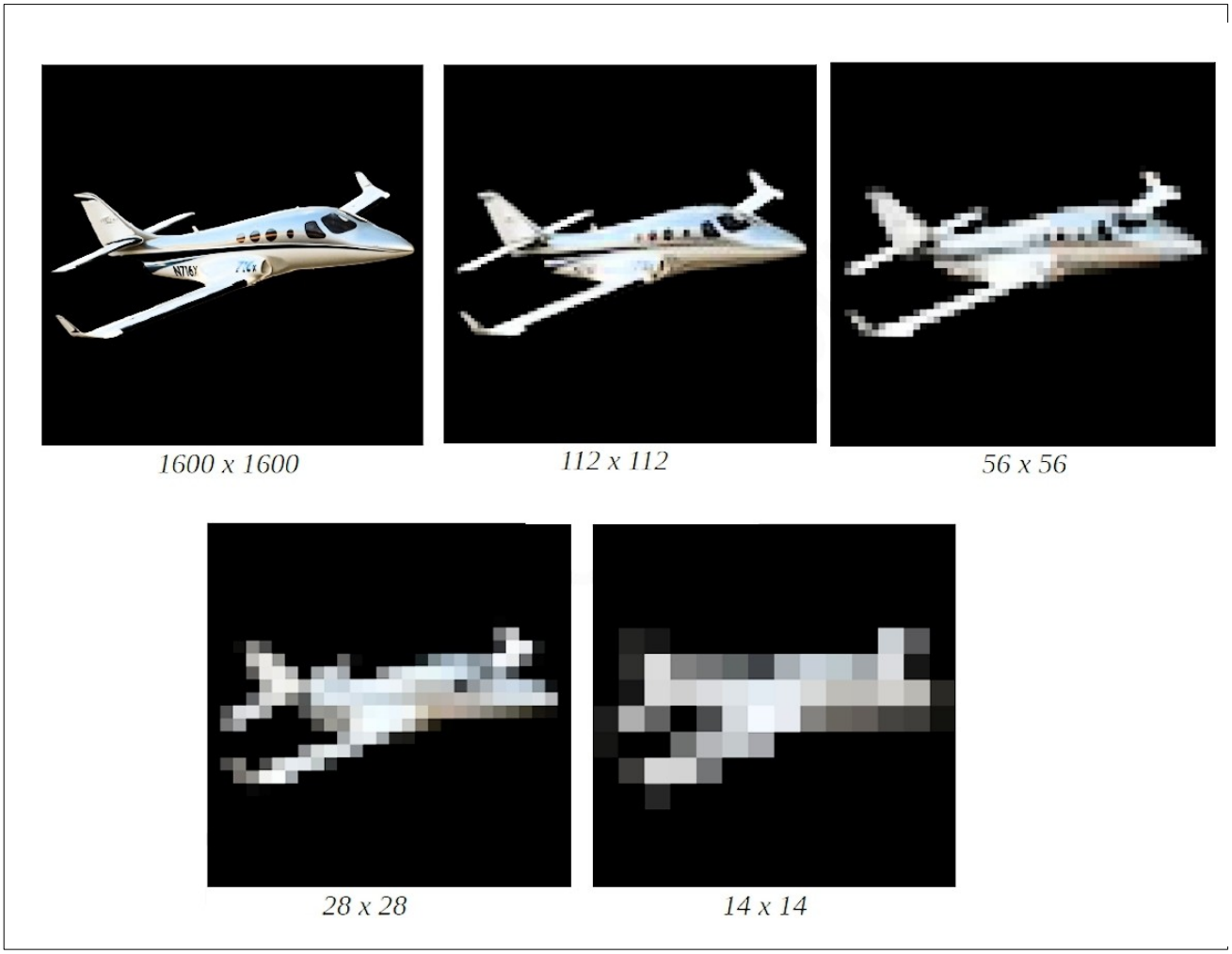

3. Estimating the object's size based on the limitations of the pixel resolution

Figure D4 shows the effect of pixel resolution on an image as the pixel resolution is reduced. It can be seen that if the object had wings that this would be noticeable even down to very low resolutions of even 23 pixels as shown in figure D3. This presents a possible way to estimate the size of the object based on how close the object was to the planes camera by estimating how many pixels an object of a given size would present for a given altitude and β angle in the horizontal dimension. Equations E1 and E3 give the ability to calculate the span distance in ft presented by the object. The span distance is directly proportional to the horizontal dimension of the sensor which 1280 pixels. We assume in the following calculations that an object with a horizontal dimension of between 21 to 22 pixels will have features that would allow for the determination of wings or some possible aerodynamic shape.

Flir Field of view Deg α	1.3	A Plane Altitude Ft	15,000.00	Altitude Increments Ft	750.00	Camera angle β below Horizon deg	-17.00
Altitude ft of Object h_i	Vert Distance From Camera to Object ft vd_i	Slant Diagonal Distance Sdd ft With α deg angle down	Field of View at Object ft or Span = Spn_i	Reticle Field of View ft	Object Size Ft	Pixel Horiz Size for with 1280 Pix Sensor 1X Magnification	Altitude ft of Object h_i
750.00	14,250.00	48,739.33	1,105.91	184.32	11.52	10.42	750.00
1,500.00	13,500.00	46,174.10	1,047.70	174.62	10.91	11.00	1,500.00
2,250.00	12,750.00	43,608.87	989.50	164.92	10.31	11.64	2,250.00
3,000.00	12,000.00	41,043.64	931.29	155.22	9.70	12.37	3,000.00
3,750.00	11,250.00	38,478.42	873.09	145.51	9.09	13.19	3,750.00
4,500.00	10,500.00	35,913.19	814.88	135.81	8.49	14.14	4,500.00
5,250.00	9,750.00	33,347.96	756.67	126.11	7.88	15.22	5,250.00
6,000.00	9,000.00	30,782.73	698.47	116.41	7.28	16.49	6,000.00
6,750.00	8,250.00	28,217.50	640.26	106.71	6.67	17.99	6,750.00
7,500.00	7,500.00	25,652.28	582.06	97.01	6.06	19.79	7,500.00
8,250.00	6,750.00	23,087.05	523.85	87.31	5.46	21.99	8,250.00
9,000.00	6,000.00	20,521.82	465.65	77.61	4.85	24.74	9,000.00
9,750.00	5,250.00	17,956.59	407.44	67.91	4.24	28.27	9,750.00
10,500.00	4,500.00	15,391.37	349.23	58.21	3.64	32.99	10,500.00
11,250.00	3,750.00	12,826.14	291.03	48.50	3.03	39.58	11,250.00
12,000.00	3,000.00	10,260.91	232.82	38.80	2.43	49.48	12,000.00
12,750.00	2,250.00	7,695.68	174.62	29.10	1.82	65.97	12,750.00
13,500.00	1,500.00	5,130.46	116.41	19.40	1.21	98.96	13,500.00
14,250.00	750.00	2,565.23	58.21	9.70	0.61	197.92	14,250.00
15,000.00	0.00	0.00	0.00	0.00	0.00		15,000.00

Figure D5: Pixel resolution vs altitude vs object size for a given Beta Angle of – 17 degrees only showing that at an altitude of 8,250 ft the object's size is 5.46 ft and its horizontal pixel resolution is 21.99 pixels

We can then write that the objects pixel resolution O_P is the ratio of the objects size to the span distance times the horizontal resolution of the sensor as show in equation E8 below:

$$O_P = 1280 * \left(\frac{O_S}{Spn} \right) \qquad \text{E8}$$

Using equations E1, E3 and E8 we derive Figure D5. For three ranges of β angles -5°, -17° and -33° we construct Figure D6, which shows at what altitudes the pixel resolution is large enough to be able to see detail in the object's image. What the table in Figure D6 tells us is that for an angle of -33° that the object must be greater than 9ft in diameter to have recognizable features, similarly for an angle of -17° the object must larger than 16 ft to be recognizable and at – 5° the object must be larger than 30 ft to be recognizable. This takes into account that the object is assumed to be at an altitude at least 3750 ft as described earlier to be higher than the San Louis Mountain range and shown in Figure A16 above. An examination of the probability distribution of the β angles is shown in Figure D7 shows that there is no centrality to the distribution and all angles are almost equally distributed in a similar fashion to a uniform probability distribution. This means all angles are equally likely to see recognizable features if close enough.

In Figure D6 the green ALL areas show the size of the object that at all altitudes would present enough pixel resolution to detect features in the object. If no features are observable then the size of the object must be less than this. As an example, in column 4 for β = -33 ° no significant features will be visible for an object less than 9 ft. Given the fact that for all angles throughout the RD2 video no images reveal any

significant detail; the object must be less than 9ft, as this satisfies the requirements for all three cases. This means that the object is small and in the range of 1ft to 9 ft in the horizontal dimension.

Object size in ft	Min Altitude for good resolution β = -5 deg	Min Altitude for good resolution β = -17 deg	Min Altitude for good resolution β = -33 deg	Acceptable Pixe resolution21-22
1.00	none	14,250.00	13,500.00	
2.00	none	13,500.00	12,750.00	
3.00	none	12,750.00	11,250.00	
4.00	14,250.00	12,000.00	9,750.00	
5.00	14,250.00	11,250.00	8,250.00	
6.00	14,250.00	10,250.00	6,750.00	
7.00	13,500.00	9,750.00	5,250.00	
8.00	13,500.00	9,000.00	3,750.00	
9.00	13,500.00	8,250.00	All	
10.00	12,750.00	7,500.00	All	
11.00	12,750.00	6,750.00	All	
12.00	12,750.00	6,000.00	All	
13.00	12,000.00	5,250.00	All	
14.00	12,000.00	4,500.00	All	
15.00	12,000.00	3,750.00	All	
16.00	12,000.00	All	All	
17.00	11,250.00	All	All	
18.00	11,250.00	All	All	
19.00	11,250.00	All	All	
20.00	10,250.00	All	All	
21.00	10,250.00	All	All	
22.00	10,250.00	All	All	
23.00	9,750.00	All	All	
24.00	9,750.00	All	All	
25.00	9,750.00	All	All	
26.00	9,000.00	All	All	
27.00	9,000.00	All	All	
28.00	9,000.00	All	All	
29.00	8,250.00	All	All	
30.00	8,250.00	All	All	

Figure D6: Object size vs beta angle and the minimum altitude for usable pixel resolution.

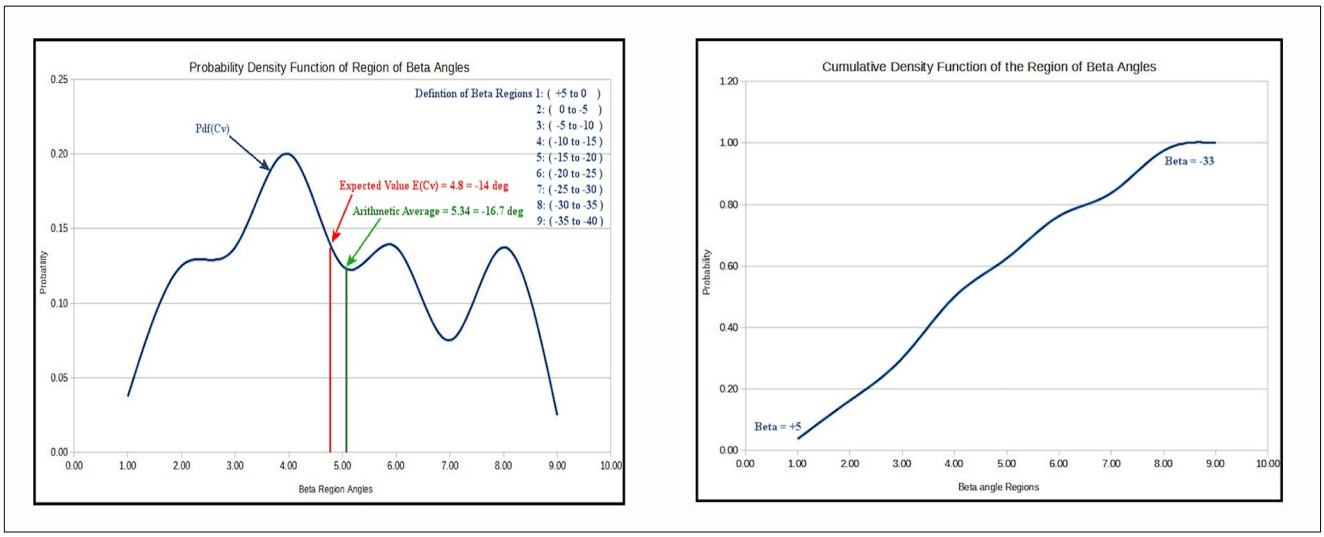

Figure D7: Probability density function and Cumulative density function of Beta angle showing close to a Uniform probability distribution.

Appendix E: Analysis of the Geographic Trajectory

1. Geographic Coordinates obtained from the 30 Sample FLIR metadata of the plane.
During the entire RD2 video the object appears to be circling over a 38 square mile area in a peculiar trajectory over the Buenos Aires National Wildlife Refuge located near the Arizona/Mexico border. 30 Samples were taken of the metadata geographical coordinates at the four cardinal points of the compass N, S, E and W to provide a locus of points that the plane had to transit to keep the object approximately centered on the screen. This is a very small area so the plane would be banking every 2 to 3 minutes to track the object as it flew its peculiar path. Table E1 shows the list of coordinates taken from the meta data used to plot the trajectory shown in Figure E1. This may account for the sinusoidal like variations in Figure A7.

1	Raw-Latitude	Raw-Longitude	Compass	Latitude	Longitude	Time Stamp
2	31.4370	26.9383	S	31.5240	-111.4490	0.4600
3	29.8196	26.9979	E	31.4970	-111.4500	1.2400
4	28.7800	26.0628	N	31.4797	-111.4344	1.4700
5	29.9791	23.7740	W	31.4997	-111.3962	2.3800
6	32.2070	26.1440	S	31.5368	-111.4357	3.4600
7	30.2804	28.0803	E	31.5047	-111.4680	4.4100
8	28.6381	26.2306	N	31.4773	-111.4372	5.2800
9	30.5260	24.1067	W	31.5088	-111.4018	6.2600
10	32.3136	26.3392	S	31.5386	-111.4390	7.3000
11	30.8511	28.2949	E	31.5142	-111.4716	8.2900
12	28.9916	26.4402	N	31.4832	-111.4407	9.1700
13	31.0964	24.0018	W	31.5183	-111.4000	10.1500
14	32.8700	26.5102	S	31.5478	-111.4418	11.1900
15	31.3404	28.3106	E	31.5223	-111.4718	12.1300
16	29.7200	26.6378	N	31.4953	-111.4440	12.5700
17	31.5185	25.0076	W	31.5253	-111.4168	13.4300
18	33.0058	26.7191	S	31.5501	-111.4453	14.4400
19	31.7104	27.6523	E	31.5285	-111.4609	15.1600
20	29.1741	26.7838	N	31.4862	-111.4464	16.0600
21	32.0023	23.8979	W	31.5334	-111.3983	17.3600
22	33.7155	26.9169	S	31.5619	-111.4486	18.5500
23	32.2783	29.9821	E	31.5380	-111.4997	20.0100
24	30.1995	26.9543	N	31.5033	-111.4492	21.0800
25	32.5654	24.5380	W	31.5428	-111.4090	22.1100
26	34.4992	27.0735	S	31.5750	-111.4512	23.1800
27	32.7599	29.6337	E	31.5460	-111.4939	24.2000
28	29.7845	27.1222	N	31.4964	-111.4520	25.3200
29	33.1088	23.9961	W	31.5518	-111.3999	27.0000
30	35.4430	27.2663	S	31.5907	-111.4544	28.2800
31	33.3806	29.7336	E	31.5563	-111.4956	29.3200

Table E1: 30 Sample table longitude and latitude values expressed in degrees and minutes into degrees and fractional degrees for map plotting applications. Only the minutes are shown as only minutes needed fractional conversion as the degrees remained constant throughout the video. Time stamp is the location in the video at minutes.seconds

As can be seen by the compass indications, the object is moving counter-clockwise in a circular trajectory S > E > N > W throughout the entire 30-minute video.

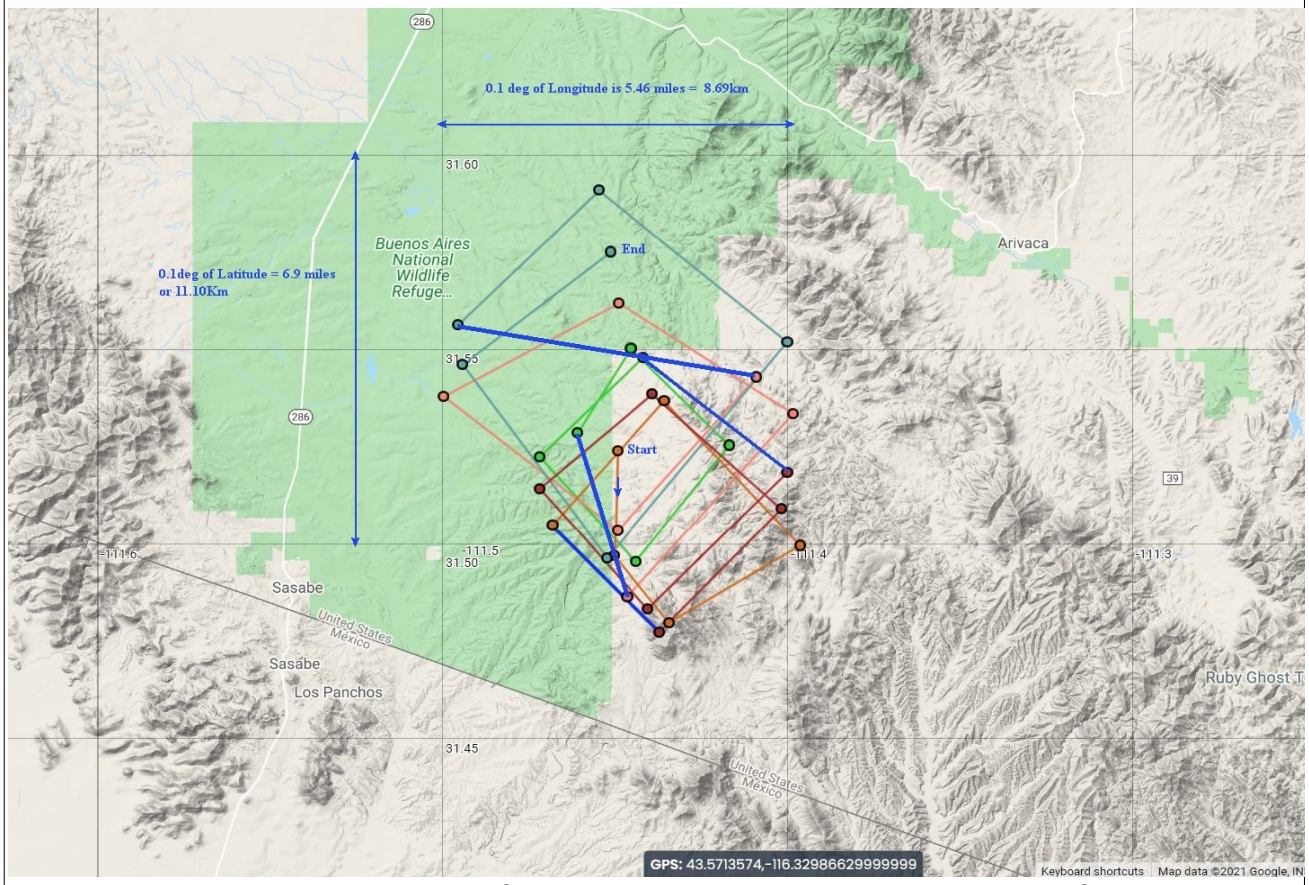

Figure E1 Object's trajectory derived from the metadata geographical coordinates from 30 samples of cardinal points of the compass during the RD2 30-minute video

Figure E1 shows 5 circular trajectories each in a different color and appearing square because they only show the compass cardinal points N, S, E and W. plotted using an online resource Map Maker **[10].** The blue lines are connectors between the different circular trajectories. The point start is the starting point of the RD2 video at a time stamp of 46 seconds into the video and the End is a time stamp at 29 minutes and 32 seconds into the video. What would be of interest in this particular area is a possible research area for future investigations. Future possible areas of investigation could include: geomagnetic or gravitational anomalies in the area. Other possible areas of investigation might be hydro-thermal and mineral concentrations. A more detailed investigation of this is out of the scope of this research investigation and will not be discussed further.

2**. Geographic Coordinates obtained from the 80 Sample FLIR metadata**

As previously described in **Appendix A Sec. 3 (p. 15)**, a second set of 80 samples were taken throughout the video to test if any under sampling of the metadata might have occurred. A plot from Google Earth Pro of the first three rotations of the object are shown in figures E2 and E3.

This was done to reduce the complexity of the image and consists of the first 25 points of the 80-sample table of Vp presented previously in **Fig. A5 (p. 15)]** that did not include the geographic coordinates. Figure E3 shows that the object passes over the outer edge of the San Louis Mountain range which is 3,750 ft high. It appears to be much higher than this attitude and so sets a lower boundary on the calculations of the objects speed shown in **Figs A11, A12 and A13 (p. 21-22)** and range of possible size values in **Fig. A16 (p. 24)** and **Appendix D, Figs. D5 and D6 (p. 38-39).** In **Fig. A8 (p. 17)** and **Fig. E2** (below), the green line shows a possible trajectory of the object as the plane tracks it in its circular path. The yellow points RV1, RV5 and RV9 show where a river repeatedly comes into view. This shows that the object is traversing a circular path and is not located in a single location because the landscape keeps changing and repeating as the river comes in and out of view. If the object were stationary or circling a small area then the same objects in the landscape would be visible from different perspectives and this is not the case. Further in **Appendix F Secs. 3-7 (p. 44-47)** the pilot's description indicates that object was traveling through the valley and against the wind for an extended period of time. This is not consistent with a stationary object or one that was confined to a small area in its movement.

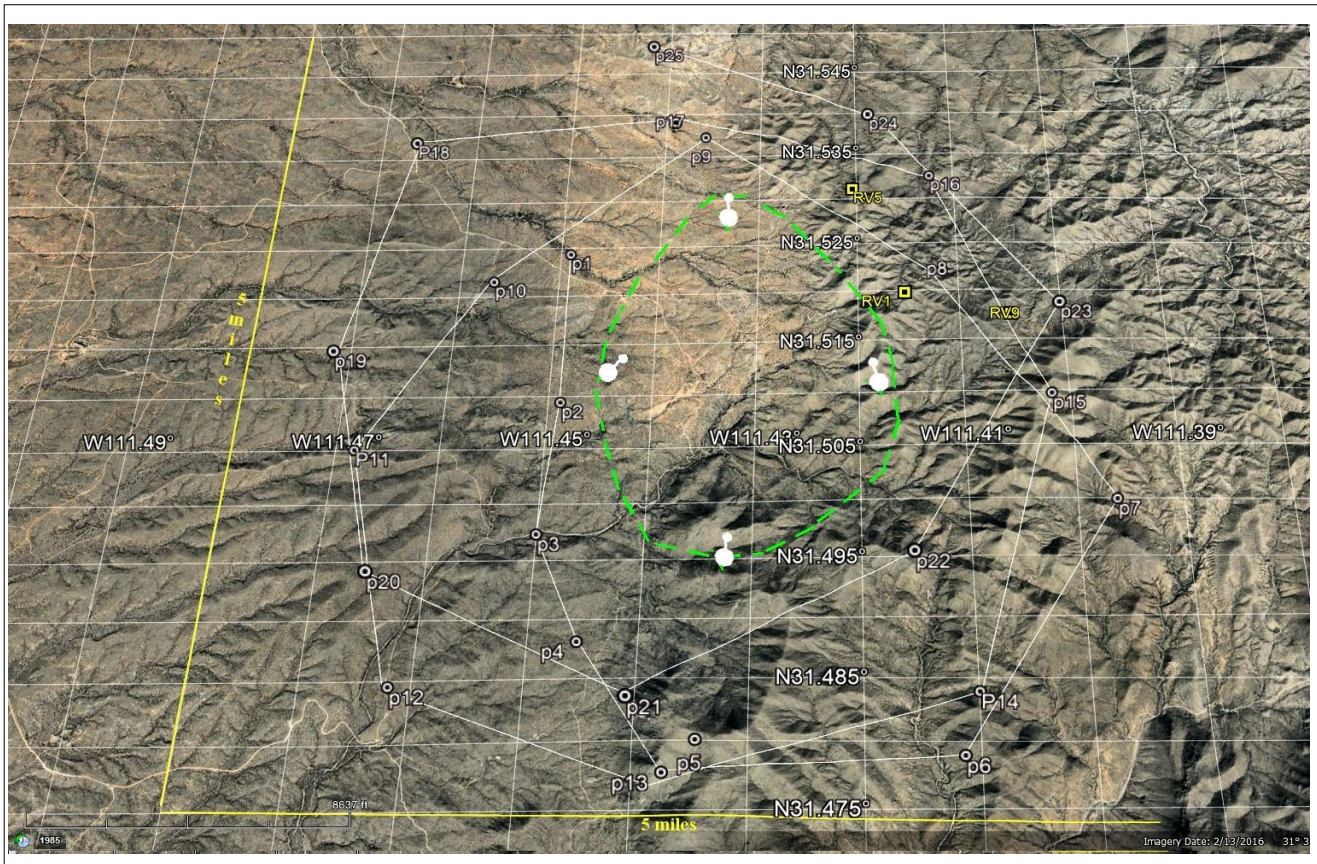

Figure E2: Plot of the first 3 rotations of the object tracked by the plane consisting of 25 sample points

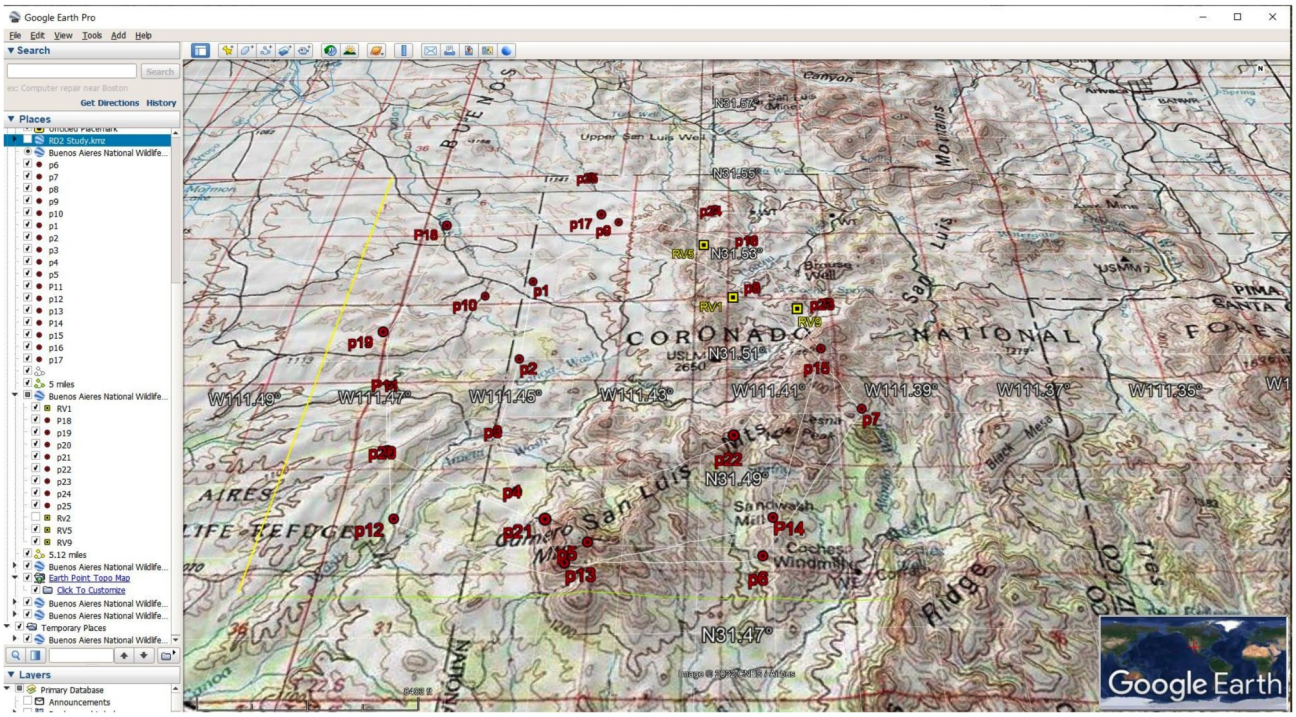

Figure E3: A high level view of the object's trajectory plotted in Google Earth Pro showing the first 25 points shown in red, of the trajectory consisting of 3 complete rotations. This perspective shows that the object passes over the westerly side of the San Louis Mountain range during the R2 video.

Appendix F: The full source anonymous description of the events surrounding the capture of the video follows.

1. SOURCE
The source wishes to remain anonymous. The source is a (redacted) US Customs and Border Patrol Agent stationed as a Tactical Paramedic for Special Operations of CBP Border Patrol (redacted) Station. The source's credentials have been verified to the aforementioned team members with Photo ID.

2. SOURCE PREPARED STATEMENT
In November of 2019, I, Border Patrol Agent (BPA) (redacted), a member of the (redacted) Sector Flight Tasked Mobile Response Team, became aware of a video that showed an unknown type of object filmed by a Department of Defense aerial asset (Arizona Air National Guard) Callsign (redacted), a RC-26 Metroliner.

One of my teammates participated aboard the (redacted) flight and filmed the video now known as the "Rubber Duck." Upon conclusion of his flight, the Agent requested a copy of the video from DOD personnel who also manned the flight. The video was placed onto a USB device and brought back to our MRT (Mobile Response Team) room for review. The video was submitted to our Sector Intelligence Unit (SIU) in a Sensitive Compartmental Information Facility (SCIF) for approximately two weeks while they (SIU) conducted their review. After being reviewed by the SIU star, it was determined NOT to have a Nexus to smuggling. The video was then released back to MRT, and I subsequently obtained an official copy. The copy was loaded onto a network shared drive with the official report filed in standard format indicated the use of a Small Unnamed Aerial System (SUAS). The video has since remained on a "shared drive" that numerous personnel within the (redacted) Sector Special Operations Detachment have access to.

That same year, I asked permission to share the video. One of my supervisors indicated that it was ok to do so and thus a limited amount of people have seen it. I did not ask permission to share it with a scientific organization and thus, it has been shared for entertainment purposes and curiosity with friends and family up until recently.

I have since flown with the crew who was part of the event, and further follow up and questioning with them suggest that they were unsure what the object was, but they assumed that it could have been a Mylar balloon or SUAS. I am not aware of any reports that they could have filed nor would I have the access to them. My teammate has declined to speak with anybody about the event due to his position within the USBP. (redacted), 6/20/21

3. SOURCE TEXT MESSAGES RE: "RUBBER DUCK" VIDEOS
"The Duck Video was filmed by my teammate on his flight…The Duck Video was immediately classified and sent to our SCIF here in (redacted). It was held for 2 weeks and then released back to us. Our intel guys analyzed and concluded that it didn't have a nexus to smuggling. Knowing that they returned it to our flight team and hence I got I copy. ***The pilots did not see it, only the Mission Sensor Operator did at the time.*** The crew on the RC-26 filmed accidentally while searching for a group of

illegal aliens. They tried to get Agents to see or get eyes on what it was, but no Agents could spot it. ***It traveled a good long while while with the RC-26 following it. They eventually ran out of flight time and gas and had to return to the guard base*** in (redacted). I talked to the MSO and he really couldn't say what it was. ***He thought it might have been a Mylar balloon but couldn't say for certain because of its behavior and shape*…(**He) wished they could have followed it further but, unfortunately, they were running out of mission time and gas. ***He did think it was odd that it seemed to be cruising through what he thought were canyons.*** **He couldn't say for sure.** ***He said the other crew members thought it might be a party balloon and left it at that despite following it for 40 minutes or so.*** They concluded that it was not a threat nor indicated criminal activity. He didn't think they reported it to anyone because the commander of the Counter Drug Unit was the Mission Sensor Operator (MSO)....camera operation for that flight. They never talked about it."

4. CAMERA

The videos are recordings from a Department of Defense FLIR Star SAFIRE 380 HD camera.

5. AIRCRAFT

The aircraft equipped with the FLIR camera that recorded the video is a RC-26B "Condor" aircraft (claimed by source and indicated by research results), tail # (redacted) According to the National Guard Incident Awareness and Assessment Handbook, 3rd Edition, the RC-26B is a Fairchild SA-227 Metro 23 twin-engine, turbo-prop aircraft. Performance and capabilities are as follows:

Air Speed	Max: +/- 248 kts Cruise: 250 kts Imaging: 140-160 kts
Operational Range	1200 NM
Endurance	Max: 6 hours Operational: 4-6 hours
Operational Altitude	Up to 30k ft; Typically 8-13k ft for Counter Drug; 2-15k ft for other missions
Sensor Type	EO/IR FMV -Color EO/IR FMV sensor -FLIR w/four fields of view -Thermal imager 3-5 micron range (no thermal crossover) -Laser Pointer -Standard Sensor resolution NIIRs 4-5; NIIRs 6 @4500 ft AGL

According to a USAF IG report on its use in protest surveillance flights in June of 2020, the RC-26B is a modified C-26 aircraft originally used by the Air Mobility Command (which is itself a modified Fairchild Metro 23 aircraft), 11 of which the Air National Guard acquired and modified in 1996 for day and night full motion video capabilities and renamed the RC-26B. While used briefly for overseas

military operations with classified sensors, these were removed and the aircraft only has the capability to record infrared and electro-optical imagery. The aircraft supports the Department of Homeland Security and various of its sub-agencies. The RC-26B is stationed at 10 operating locations, including (redacted), where it is used by the (redacted) Air National Guard to support U.S. Customs and Border Protection operations. The aircraft has 3 crew members; 2 pilots and 1 Mission Systems Officer (MSO), who operates the onboard sensor and ground communications equipment. According to the same USAF IG report, the RC-26B was chosen for the protest surveillance mission in June 2020 "… along with its capability to provide forward looking infrared (FLIR) and optical/infrared (EO/IR) full motion video" (Report of Investigation (S8934P) RC-26B Operations 1-4 June 2020, The Inspector General Department of the Air Force). Of note, U.S. Representative Adam Kinzinger is a RC-26B pilot.

Aircraft and UAP Flight Data… (Redacted can help determine speed, heading, size, acceleration)

6. UAP ANOMALOUS CHARACTERISTICS

The primary anomalous characteristic of the UAP displayed in the videos is the fact that the UAP IR signature is white/cold while the FLIR camera setting is black/hot. **[Appendix B p.32 Item 8, (9)]**
Any conventional aircraft, including high-performance drone, would generate a heat signature from the combustion engine or electric motor or battery. This primary anomaly was also noted in the field report below of the aircrew which filmed the UAP; ***"The SUAS was not giving off any heat signature…."***

The second anomalous characteristic of the UAP displayed in the video is its shape. It does not match any known small unmanned aerial system (SUAS). The shape of the UAP was also noted by the aircrew in their report below; "… ***it appeared to be a circle towing a smaller circle underneath it."***

The third anomalous characteristic of the UAP displayed in the video is its speed. The characteristic was also noted by the aircrew: the UAP "… did fly into the wind without difficulty."

7. CPB FIELD ENCOUNTER REPORT

CBP (redacted) Field Encounter (Unclassified/FOUO)

Report Title:
Family Unit Alien group used a diversionary tactic for a small unmanned aerial system incursion into U.S.
Date and Time of Information:
11/23/2019 00:33

Executive Summary:

On November 23, 2019, after the apprehension of a Family Unit Alien group of 92 illegal aliens in Border Zone (redacted) Area of Responsibility, ***an Army National Guard air asset spotted a small unmanned aerial system (SUAS) making an incursion into the United States from Mexico.*** TUS agents were unable to respond to the UAV due to the apprehension of the FMUA. Additional air assets were unable to respond to the area when the Army National Guard air asset had to return to base at 02:52 hours.

Narrative:

On November 23, 2019, at approximately 00:33 hours, the (redacted) Station (TUS) Common Operating Picture (COP) camera operators observed a large group of subjects illegally enter into the United States in Border Zone (redacted). At approximately 01:09 hours, TUS agents responded and apprehended the Family Unit Alien (FMUA) group of 92 without incident (ref. (redacted)).

A National Guard air asset, (redacted), was in the area when the FMUA group was apprehended and began to scan the surrounding area to check for any illicit traffic using the large FMUA group as diversion. At approximately 02:01 hours, the TUS Tactical Operations Center (TOC) Supervisor was notified that (redacted) had visual of a small unmanned aerial system (SUAS) carrying what appeared to be a package at coordinates N 31.479833, W -111.4215. The SUAS was observed between Cumero-Mountain and Fresnal Wash, approximately three miles northeast of where the FMUA group was apprehended.

At 02:06 hours (redacted) provided a third and final coordinates of the SUAS of N 31.594667, W 111.479167, ***approximately 1.5 miles due east of Arivaca Lake. (redacted) advised that the SUAS was flying a slow back and forth pattern and that it appeared to be a circle towing a smaller circle underneath it. The SUAS was not giving off any heat signature but did fly into the wind without difficulty.***

(redacted) had to return to base shortly after their final update (NFI). No other air assets were amiable to help in the search for the SUAS when (redacted) had to terminate. Mobile Surveillance Capabilities (MSC) and COP operators were unsuccessful assisting in locating the SUAS for the duration of the search or after (redacted) had to terminate.

References

https://s3.documentcloud.org/documents/3219687/U-S-National-Guard-Incident-Awareness-and.pdf
https://www.globalsecurity.org/intell/systems/rc-26.htm
https://www.youtube.com/watch?v=vY7ckdeCYqo
https://tinyurl.com/39hv3e7p
https://www.azmirror.com/blog/what-we-know-about-the-national-guard-plane-that-surveilled-protests/

https://www.youtube.com/watch?v=gCdnyOBzb-I
https://www.youtube.com/watch?v=XE4y3PArOmw&t=138s

Location, Heading, and Speed of CBP Aircraft with UAP in frame

	TIME	LAT	LONG	HDG	SPD
Video 1					
Begins:	08:41:40Z	31º 29.79’ N	111º 22.97’ W	290º T	202 KTS
Ends:	08:50:58Z	31º 30.12’ N	111º 24.30’ W	328º T	175 KTS
Video 2:					
Begins:	08:50:59Z	31º 30.17’ N	111º 24.33’W	328º T	175 KTS
Ends:	09:20:58Z	31º 31.85’ N	111º 29.67’ W	165º T	204 KTS